Title: Olfactory memory consolidation requires the TRPV channel OSM-9 in sensory neurons of the circuit.

Kelli L. Benedetti[1,*], Fatema A. Saifuddin[1,*], Julia M. Miller[1,#,] Rashmi Chandra[1,#] Alec Chen[4,], Raymond L Dunn[1], Julia A. Kaye[5], Bo Zhang[6], Saul Kato[7], Maria E. Gallegos[8] and Noelle D. L'Etoile[1,+]

[1]Department of Cell and Tissue Biology, University of California, San Francisco, San Francisco, CA, United States of America

[4]Lowell Science Research Program, Lowell High School, San Francisco, CA, United States of America

[6]Washington University, Department of Pediatrics, School of Medicine, Washington University in St. Louis, St. Louis, MO 63130, USA

[7]Department of Neurology, University of California, San Francisco, San Francisco, CA, United States of America

[8]Department of Biological Sciences, California State University East Bay, Hayward, California, United States of America

[5]Gladstone Institute of Neurological Disease, Gladstone Institutes, San Francisco, CA, United States of America

[*.] Co-first authors

[#.] Co-second authors

[+]Corresponding author

Email: noelle.letoile@ucsf.edu

Abstract

Memory is one of the most important abilities of the brain. It is defined as an alteration in behavior as a consequence of an experience. For example, the *C. elegans* nematode will downregulate its chemotactic response to the innately attractive odor, butanone, if the odor is not paired with food. Through repeated, spaced training with this odor in the absence of food, *C. elegans* will maintain this memory for a prolonged period of time. Although transient receptor potential (TRP) channels are classically thought of as primary sensory receptors, it was reported that the OSM-9/TRPV5/TRPV6 (TRP vanilloid 5/6) channel is required for single exposure learning. Here we describe a new role for *osm-9* in consolidation of memory that is induced by repeated, spaced training. In this paradigm, *osm-9* mutant animals learn as well as wild-types, but are unable to consolidate the memory. Though sleep is required for memory consolidation, loss of the TRPV channel OSM-9 does not affect sleep. This indicates that the TRP channel promotes memory in a process that acts outside the sleep pathway. We investigate the endogenous expression pattern of OSM-9 and show that it is not expressed in the butanone-responsive AWC olfactory sensory neuron. Instead, it is expressed in the paired AWA olfactory neuron, the ASH nociceptive neurons, the OLQ and two other unidentified sensory neurons which are most likely ADF and ADL as they express *osm-9* mRNA. Because OSM-9 acts in sensory neurons that do not participate in butanone sensation, this indicates that the circuit participates in olfactory memory consolidation.

Introduction

Learning and memory are vital to survival. Organisms must update their knowledge of their surroundings based on environmental cues. One such way to promote learning and memory is through neural plasticity, which involves changes at the structural, molecular, and functional levels. Pioneering studies on the *Aplysia* gill-withdrawal reflex demonstrated the importance of synaptic plasticity on learning and memory through *in vitro* pharmacology and physiology experiments [1]. Learning and memory are thought to be driven by two types of synaptic plasticity: the first is Hebbian, which includes synaptic long-term potentiation (LTP) and long-term depression (LTD) [2], and the second is synaptic scaling a non-Hebbian homeostatic compensation, which allows a system to return to baseline [2,3]. A large number of molecules implicated in these processes include factors that reorganize the actin cytoskeleton, affect trafficking, insertion and localization of receptors and cell adhesion molecules, localization of newly translated products, kinase function, and transcription of new genes [4]. As molecular as, our understanding of these synaptic processes may be, we are still missing the roles of some molecular players for memory in any intact organism. One protein type that is gaining new evidence for its role in memory is the TRP channel.

Transient receptor potential (TRP) ion channels were first discovered in the *Drosophila* eye photoreceptor cells [5-7], but have since been found in mammals and even in the single-celled yeast. Classically, TRP channels have been well established as magnesium-, sodium-, and calcium-permeable cation channels that can be activated by and simultaneously integrate multiple intracellular or extracellular stimuli to drive downstream signaling and membrane depolarization. These stimuli include, but are not

limited to, pain, temperature, pH, injury, osmolarity, and cytokines [8]. There are seven TRP channel families, all sharing a similar topology, with six transmembrane helices, a short pore helix, and a cation-permeable pore loop region. The TRP families are distinguished by how many N-terminal ankyrin repeat domains they have and other they have a tC-terminal TRP box helix, which is a C-terminal helix parallel to the membrane [9]. The TRP vanilloid-type (TRPV) family members with six ankryin domains and TRP box helix are generally considered as first-line nociceptive sensory receptors. TRPV1 is stimulated by vanillin, vanillic, endogenous lipids like the *N*-acylamides (e.g. endocannabinoids such as anandamide), high temperature (≥43°C), pain, ethanol, low pH, black pepper, garlic (allicin), cannabidiol (CBD), arachidonic acid, resiniferatoxin, and capsaicin in spicy foods [8-11]. The six ankyrin repeats in TRPV1 each contain two short anti-parallel helices and a finger loop and have been shown to interact with the proteins calmodulin and PI3K [9,12]. Upon activation, the TRPV1 channel allows calcium ions to enter the cell at the plasma membrane through the pore loop region, ultimately leading to desensitization of the channel and a subsequent refractory period [9]. Taking advantage of this desensitization may allow therapeutic intervention to alleviate acute and chronic pain. Although the sensory role of TRPV proteins has been well established, other roles of the TRPV channels, including the promotion of neural plasticity required for memory formation, remain unclear.

TRP channels have more recently been studied for their role in the central nervous system, including neural plasticity [14]. For example, TRPV channels are expressed in the hippocampus where they have been implicated in slow synaptic transmission [15], LTP [16], and LTD [17]. Though TRPA channels are required for

nociception and cold sensing [8], the TRPA channel (*painless*) is also required for the neuroplasticity underlying fly courtship and associative long-term memory [18]. In the mammalian brain, TRPCs function in the hippocampus to drive synaptic transmission and plasticity, and subsequent spatial working memory [20,21]. In addition to the hippocampus, expression of TRPCs has been seen in the temporal lobe, suggesting a role in neural plasticity, learning, and memory. Likewise, TRPM4 is expressed in the mammalian hippocampus and is important for plasticity and spatial working and reference memory [22]. Several studies have implicated mammalian TRPV1 in memory formation, including fear memory consolidation behavior in mice [16,23,24]. Acute stress was found to block spatial memory retrieval in young rats and also blocked LTP and drove LTD in CA1 slices of the hippocampus, whereas TRPV1 agonists allowed spatial memory and LTP while blocking LTD, even in the presence of stress [24]. These TRPV1 memory studies were done with either pharmacological agent infusion to activate TRPV1 or by studying the behavior of TRPV1 knockout mice. Further dissection of the exact cellular or molecular interactions occurring in the behaviorally-defective mice will provide a mechanistic understanding of how learning and memory are driven. An outstanding question is which stage of memory formation is mediated by TRP channels: acquisition, consolidation, or recall? In order to study the required genes in a live animal model as it is behaving, unbiased screens for genes required for learning and memory would need to be performed.

The *C. elegans* nematode exhibits olfactory classical conditioning: prolonged exposure to innately attractive food-related odors in the absence of food elicits a

downregulated response to the odor [25]. The *osm-9* gene is required for short-term olfactory memory in this paradigm. However, the mechanisms and dynamics of TRPV function in long-term memory formation [26,27] remain unknown. In addition, a role for *osm-9* in long-term memory has not been reported. Examination of the mechanisms and dynamics underlying TRPV-mediated memory in live *C. elegans* would help us understand how these channels act to integrate signaling over time to promote memory formation in a behaving animal.

C. elegans provides a good model system to approach this problem. It is genetically-tractable and its nervous system is comprised of 302 neurons connected via 7,000 synapses. Also, it is the only organism where the entire connectome has been mapped [28,29], whereas the mammalian nervous system has 100 billion neurons connected by trillions of synapses and the entire neural connectivity map remains unknown [30]. Additionally, it can form long-term associative memories of olfactory stimuli [26]. Furthermore, the neural circuit underlying olfaction is well established [28,31,32]. Importantly, it is transparent, making live cell imaging in the live animal a possibility. Thus, studying plasticity in the olfactory circuit in *C. elegans* has the potential to give us insight into the mechanisms by which experience changes complex neural circuits to promote memory formation.

The *osm-9* gene is an ortholog of human TRPV5 and TRPV6. TRPV5 and TRPV6 are not like the rest of the TRPV family, as they are not ligand-gated, nor are they thermosensitive [33,34], and are highly-calcium selective [35]. TRPV5 and TRPV6

are localized to epithelial cells in the kidney and intestine [36] and are constitutively open at physiological membrane potentials and are modulated by calmodulin in a calcium-dependent manner [35]. Initially, *osm-9*/TRPV5/TRPV6 was discovered in a screen for *C. elegans* mutants defective for sensing high osmolarity. It was subsequently studied for its role in diacetyl chemotaxis as well as short-term associative olfactory memory in which the nematodes learn to ignore food-related odors when they are encountered in the absence of food [25,37]. In the nociceptive neuron, ASH, OSM-9 is required for SDS avoidance [38]. Polyunsaturated fatty acids, including the putative TRPV1 endogenous activator arachidonic acid, may function upstream of *osm-9* to mediate sensory transduction [40]. The endogenous agonist nicotinamide was discovered to activate an OSM-9 and OCR-4 heteromer expressed heterologously in *Xenopus* oocytes, and nicotinamide was sufficient to stimulate endogenous behaviors mediated by OSM-9 [41]. The *osm-9* gene has also been shown to play a role in developmental programming and is downregulated transcriptionally post environmental stress exposure, causing avoidance of specific olfactory cues [42,43]. These changes in *osm-9* expression were shown to be mediated by chromatin remodeling and endogenous siRNA pathways [43]. Thus, similarity to TRPV1, *osm-9* has roles in sensory transduction in response to noxious stimuli, can be activated by polyunsaturated fatty acids, and plays a role in learning and memory.

In our classical conditioning paradigm, we focus on the *C. elegans* response to the food-related odorant butanone, which is specifically sensed by the AWC olfactory sensory neurons (OSNs) [44,45]. The *C. elegans* nematode exhibits olfactory classical

conditioning: one 80-minute exposure cycle to butanone in the absence of food causes the nematode to downregulate its chemotactic response to that odor. The second messenger for odor sensation within the AWCs is cGMP [46,47]. Prolonged odor stimulation leads to AIA interneuron circuit activity and PI3K signaling to the AWC neurons to drive accumulation of the cGMP-dependent protein kinase EGL-4 [48] within the AWC nucleus. These events promote memory of the odor being profitless after 80 minutes of conditioning [31,49,50]. Loss-of-function mutations in *osm-9* cause defective learning that AWC-sensed odors can be profitless, and defective chemo-, osmo-, and thermosensation promoted by other sensory neurons [37]. Importantly, loss of *osm-9* restores function to mutants that ignore AWC-sensed odors as a consequence of expressing nuclear EGL-4. After EGL-4 nuclear translocation, nuclear endogenous RNAi promotes a dampened response to butanone by transcriptionally-downregulating the *odr-1* gene through heterochromatin remodeling via *hpl-2/HP1*, and the *osm-9* gene is epistatic to gain-of-function *hpl-2* or *egl-4* [49,51]. Thus, the TRPV channel *osm-9* is required downstream of both of these nuclear events to block chemotaxis and is thus the most downstream component of this paradigm currently known. However, the role of *osm-9* in this plasticity paradigm is still poorly understood. We were also curious if *osm-9* plays a role in long-term olfactory memory since its role in short-term olfactory memory is established. We wanted to identify the time during which the *osm-9* gene is required for long-term memory formation, and which of its structural components allow this plasticity.

We previously found that the 80-minute butanone conditioned response is temporary and is lost after only 30 minutes recovery on food [27]. However, after odor spaced-training, *C. elegans* can exhibit long-term aversive memory phenotypes [27,52]. Worms subjected to three cycles of 80-minute exposure to the unprofitable odor in the absence of food with recovery periods on food in between each cycle will keep the memory and continue to ignore the odor for much longer periods of time (at least 16 hours after training) [27]. Here, we find that the *osm-9* null mutants can actually be conditioned to ignore butanone after undergoing a spaced-training protocol, just like wild-type animals. Interestingly, we show that long-term memory consolidation, and not acquisition, requires *osm-9,* independent of sleep. Specifically, we find that *osm-9* mutants lose this odor memory after only 30 minutes, where it remains lost. The wild-type animals also lose the memory after 30 minutes, but regain it and keep it for at least 16 hours [27]. The wild-type trained animals undergo a period where the odor memory is fragile and is lost after only 30 minutes of recovery on food, only to be regained at 120 minutes of recovery and to last for at least 16 hours. The *osm-9* mutants lose the memory at 30 minutes, however, it remains lost at 120 minutes, during which wild-type worms consolidate the memory, and it remains lost at 16 hours after training. Memory fragility in the period after conditioning is a hallmark of consolidation [53,54]. Thus, *osm-9* likely plays a role in olfactory long-term memory consolidation in addition to its previously defined role in short-term memory acquisition [25]. We previously found that wild-type nematodes, like mammals, require sleep during this fragile memory period to consolidate odor memory, but *osm-9* animals sleep just as much as wild-type, though they are unable to consolidate memory. We also find that the N-terminus of OSM-9, but

not the C-terminus, is required for long-term memory acquisition, since removing most of the C-terminal tail does not affect memory. By using CRISPR to add a GFP and and auxin initiated degradation signal to OSM-9, we find that OSM-9 is not endogenously expressed in AWC, the butanone sensing neuron, instead, it is seen in the sensory neurons: ASH, OLQs, AWA and two others in the head as well as the phasmids PHA and PHB as well as PVQ.

Though TRP channels have been extensively studied as sensory receptors, they have not been well studied as integrators of prolonged stimulation. The goal of this work was to understand how the *osm-9* TRPV channel mediates long-term memory after prolonged exposure to odor, thereby elucidating TRP function in signal integration triggered by extended exposure to stimuli. We show that *osm-9* is important for the long-term memory consolidation step of memory formation. These data suggest the exciting possibility that a TRPV channel promotes long-term memory consolidation by acting in the sensory neurons of the circuit.

Results

Although it has been previously shown that *osm-9* is required for olfactory short-term memory of food-related odorants (Fig 1, S1 Fig), its role in long-term memory formation has not been reported. We utilized a long-term memory spaced-training paradigm in which we performed odor conditioning in three spaced intervals with recovery periods on food in between (S1 Fig). We tested *osm-9(ky10)* null mutants versus wild-type animals and found that although *osm-9(ky10)* animals are unable to form short-term odor memory after one cycle of conditioning [25] (Fig 1), they can

acquire memory immediately after spaced-training, like wild-type animals (Fig 1), shown by a drop in the chemotaxis and learning indices (Figs 1A and 1B). This indicates that though *osm-9(ky10)* animals may be unable to form short-term odor memory, they can acquire long-term memory through spaced training (Fig 1). Wild-type animals lose the memory after 30 minutes of recovery on food, but regain it after two hours of recovery (Fig 2) [27], and keep it for at least 16 hours post training (Fig 3). By contrast, *osm-9* animals lose the memory after only 30 minutes (Fig 2) of recovery on food and never gain it back, as shown by the chemotaxis indices at two and 16 hours of recovery after training (Figs 2 and 3, respectively). This could indicate that *osm-9* is responsible for memory consolidation, but not acquisition. Also interesting to note is that although *osm-9(ky10)* animals are able to acquire memory after three cycles of odor training, their chemotaxis behavior looks distinct from wild-type animals – *osm-9(ky10)* animals have an average chemotaxis index closer to zero (0.1, Fig 1A), which looks like wild-type animals after one-cycle of odor training (Fig 1A). By contrast, wild-type animals show an aversion to butanone after three cycles of odor training, with an average chemotaxis index of -0.3 (Fig 1A). This may indicate that *osm-9* is required for the repulsion induced after odor training. Although odor spaced training can induce memory acquisition in *osm-9(ky10)* animals as opposed to training them with one odor cycle, their behavioral state may be different from that observed in wild-type animals.

Since sleep has been suggested to promote memory consolidation and is required for long-term memory in our paradigm [27], we asked if the *osm-9(ky10)* mutants sleep after spaced training by quantifying their quiescence behavior in the hour following spaced training. To analyze movement, we utilized the WorMotel [55], where

we could take videos of individual worms as they recover for one-hour post training, and subsequently analyzed their behavior with a Matlab script. We measured sleep by quantifying quiescence behavior which lasted longer than 30 seconds and generated raster maps from these data (Fig 4A). We then recorded the mean total quiescence (in minutes per hour) of each dataset. The *osm-9(ky10)* movements showed the same amount of quiescence as wild-type animals, signifying that the *osm-9(ky10)* animals sleep just like wild type animals, but are still unable to consolidate olfactory memory (Fig 4B).

We next tested extra *osm-9* alleles to uncover if this olfactory long-term memory consolidation defect is unique to the *osm-9(ky10)* allele, and as a way to perform structure-function analysis. The *osm-9* gene has fourteen exons. The *ky10* allele has an early stop codon at the beginning of the fourth exon from the 5' end, occurring in the middle of the third ankyrin repeat (Fig 5A). We tested the *yz6* allele, also an early stop codon, occurring at the end of the fifth exon, 3' of the six ankyrin repeats. This allele would thus leave the repeats intact, assuming the mRNA is translated (Fig 5A). We also examined the *ok1677* allele, a deletion of the twelfth, thirteenth, and part of the fourteenth exons, removing most of the C-terminal intracellular tail, and the sequence that produces a non-coding RNA and tRNA (Fig 5A). The *yz6* and *ky10* animals showed similar behavior with respect to memory acquisition, consolidation, and maintenance, (Fig 5B). The *ok1677* animals had wild-type memory, indicating that the C-terminus is not required in this memory paradigm. Thus, *osm-9* is required for integration of odor with a negative experience (starvation) over time. In addition to integration, studies with

the *ky10* allele revealed a role for *osm-9* in primary odor sensation [37]. Therefore, we asked if these additional alleles also play a role in primary odor sensation. The *osm-9* gene is required for diacetyl (2,3-butanedione) chemotaxis, which is mediated by the AWA olfactory sensory neurons. We found that similar to *ky10 and yz6* showed defects in diacetyl chemotaxis, by contrast, *ok1677* was able to chemotax well (S3 Fig). Thus, the N-terminus and not the C-terminus is also required for diacetyl chemotaxis. These data also show that the non-coding RNA and tRNA are not required for long-term aversive butanone memory nor for diacetyl chemotaxis. This work indicates that *osm-9* is indeed not required for three-cycle-induced memory acquisition, but that the N-terminal region is important for memory consolidation in long-term olfactory memory.

We next wanted to understand what cells OSM-9 is required to act within to allow consolidation of butanone memory. Thus, we tagged the endogenous *osm-9* locus with GFP and and auxin inducible degron (AID) (**Figure 7A**). To understand if the tagged version is functional, we asked whether auxin-mediated degradation of *osm-9(py8)* would phenocopy the o*sm-9(ky10)* allele. If it does, then the wild type function of the in the absence of either auxin or TIR1 would indicate that the tagged version is functional. Thus, we crossed the strain that expresses auxin E3 ligase substrate recognition subunit, TIR1, from a ubiquitous promoter. We exposed these and control animals to a titration of auxin for 30, 60 and 120 minutes and found that in the absence of auxin, *osm-9(py8)* animals were able to chemotax as well as wild types to diactyl (Figure 7B). Auxin does not affect wild type animals ability to respond to dactyl but 1mM auxin was sufficient to cause *py8* to phenocopy *ky10*, even after as little as 30 minutes exposure.

Thus, *osm-9(py8)* is fully functional in the absence of auxin and neither the GFP or AID tag affect its function in dactyl chamotaxis.

We found that *osm-9(py8)* is expressed in four neurons whose cell bodies are close to the anterior bulb of the pharynx which we identified as OLQs, AWA, ASH and two other head neurons that cluster with ASH and AWA (Figure 8B-E). As might be expected for a membrane protein, o*sm-9(py8)* staining is excluded from the nucleus (Figures 8B-E) and travels in packets anteriorly from the cell body to cilia (R.C., personal observations). We had previously postulated based on promoter fusion experiments (37) that OSM-9 may function in the AWC sensory neuron to allow odor adaptation and olfactory learning. Unexpectedly, *osm-9(py8)* is not expressed in this sensory neuron as the OSM-9::GFP does not colocalize with p*odr-1*::RFP with is expressed in AWC and AWB neurons (Figure 8C). Thus, we postulate that OSM-9 must function in the circuit to allow for olfactory adaptation and consolidation.

Discussion

Transient receptor potential (TRP) channels are proteins best understood in their role as sensors of harmful environmental stimuli, yet their role in regulating neural plasticity—a fundamental process in the brain that governs information storage and adaptation to environmental cues is more enigmatic. We found that the *osm-9* TRPV channel, which has a known role in short-term olfactory learning [25], We were curious if *osm-9* also plays a role in long-term olfactory memory, and thus tested the mutants in a spaced-training paradigm that induces long-lasting memory in wild-type animals. The *osm-9(ky10)* mutants were able to acquire the odor memory after training, but lost it

within 30 minutes of recovery on food, and never regained the memory, whereas wild-type animals lose the memory at 30 minutes of recovery, regain it two hours later, and keep it at least 16 hours later. Thus, we have discovered that the *osm-9* TRPV channel is required for memory consolidation, a key component of long-term memory. Properly functioning TRPV channels may be necessary to drive the synaptic plasticity required for memory formation. Studies have shown that TRPV1 contributes to synaptic plasticity, specifically LTD induction across the hippocampus, medial prefrontal cortex (mPFC), and nucleus accumbens (NAc) [17,56-58]. Because these are regions required for long-term memory formation, this alteration in synaptic plasticity may be required for proper memory consolidation. How OSM-9 acts non-cell autonomously, is at the moment unclear.

We observe that *osm-9* animals fail to acquire odor memory after one cycle of training, but can acquire odor memory after three-cycle spaced training. After one cycle of butanone training in the absence of food, the worms are no longer attracted to the odor (chemotaxis index is close to 0.1). However, after three cycles of training, the worms are now repulsed by the odor (chemotaxis index is close to -0.3). Because we have not directly examined if there is a difference in *osm-9* function in both one-cycle-induced short-term and three-cycle-induced long-term memory, it could be that the mechanism in each is distinct. Nuclear functioning genes, including the *egl-4* PKG and *hpl-2* HP1 homolog, act upstream of *osm-9* in one-cycle induced short-term memory function and each was shown to act in the AWC neuron [49,51]. The GFP tag on *osm-9(py8)* reveals that OSM-9 is not expressed in the AWC neuron. Thus, OSM-9 must act downstream of these factor and in a non-cell autonomous fashion to promote

odor adaptation. The highest level of *osm-9* mRNA (GenGen) is present in the ADF and ASH sensory neurons which mediate repulsion [59]. It is possible that *osm-9* is required in these neurons to engage an aversive brain state that drives memory consolidation of the odor. Conversely, it could be required in repulsive sensory neurons for the animal to understand that it is a negative cue, and subsequently the transmission to interneurons in a pattern that reflects repulsion may be necessary for integration and consolidation and memory of these negative cues.

Animals must respond to and learn from their ever-changing surroundings to ensure survival. TRP channels emerged early in eukaryotic evolution to allow sensation of the environment. Over the course of evolution, they became coincidence detectors, sensing a range of mechanical to chemical cues, which are vital for learning and memory. Originally thought of as only having peripheral nerve expression, TRPV channel proteins are also found in the central nervous system throughout the brain. Could pleiotropy be occurring, where TRPV channels in the sensory neurons can respond to cues such as heat and protons, and subsequently drive learning and long-term memory of those cues in the brain? The evolution of TRP channels could have potentially driven survival through ambient sensation and simultaneous or subsequent triggering of memory formation.

TRP channels are found throughout the domain Eukaryota, in the animal, fungi, and protist kingdoms, meaning that they evolved before multicellularity. TRPY1 is found in the single-celled fungus, *S. cerevisiae* and TRPA, C, M, L, and V channels, are found

in the single-celled protist choanoflagellates [60], as well as in multicellular, bilaterally-symmetric animals, including protostome ecdysozoan invertebrates such as *Drosophila* and *C. elegans*, and deuterostome chordate vertebrates, including zebrafish, whale and Australian ghost sharks, rodents, and humans (http://ncbi.blast.gov). TRPNs are found in *Hydra magnipapillata,* which is the last common ancestor of Cnidaria and Bilateria. Fourteen TRPA and TRPML channels were found in the sponge *A. queenslandica*, showing a diverse conservation of TRP channels since sponges are the oldest living metazoan phyletic lineage, diverging from other metazoans ~600 million years ago [60]. TRPA1 was found to have evolved from a chemical sensor in a common bilaterian ancestor to invertebrates and vertebrates, conserved across ~500 million years of evolution [61]. TRP channels themselves are likely even older than the nociceptive family of sensors, since fungi branched off from other life during the Proterozoic Era, about 1.5 billion years ago [62]. These early TRP channels evolved the ability to sense multiple stimuli and drive distinct responses to ensure organismal survival. For example, the TRPA1 channel likely evolved through adaptive evolution via amino acid changes in response to the environment, explaining the temperature and compound sensitivities observed in different mammalian species [60,63-65]. The TRP channel predecessors were non-neuronally expressed, but as animals became more evolved, such as through development of a neural net or cephalization, TRP channels evolved neuronal roles such as sensory perception and polymodality. However, the distinct functions of TRP channels in higher level processes such as plasticity, learning, and memory are still being uncovered.

Since TRPV channels are required for acute sensation and in plasticity, considered short and long-term processes, respectively, then how does its function and regulation differ between them? Distinct from the TRPV1-4 channels, TRPV5 and TRPV6 are highly-selective for calcium and mediate calcium signaling through constitutive opening at physiologic membrane potentials, without the need for ligand activation. Potentially, the TRPV5 and 6 ortholog OSM-9 may also be constitutively open and mediating the calcium homeostasis necessary to drive long-term memory formation. Calcium is a known requirement for synaptic transmission. We previously showed that synaptic plasticity occurs in animals that maintain the memory and that slept post spaced-training [27]. Another confound is understanding how TRPV1 mediates long-term memory. TRPV1-4 channel agonists cause a downstream signaling cascade to mediate sensation. Prolonged exposure causes desensitization of the channel. If the channel is similarly desensitized in plasticity, then how does its function continue to occur for long-term biological processes, including long-term memory? Understanding the agonists driving TRPV1-mediated plasticity that do not cause desensitization of the channel may help to answer this confounding question. The polymodality of TRP channels is alluring, yet mystifying since it can be a number of individual or combinations of agonists or antagonists driving varied downstream responses. Yet, since Ca^{2+} signaling is important for synaptic plasticity, it could be that TRPV proteins are specifically required for regulating intracellular calcium to promote plasticity and thus learning and memory.

Besides being a current focus for chronic pain treatment (e.g. through topical capsaicin), the TRPVs are also emerging as a new drug target for diseases affecting neural plasticity. Indeed, a vast array of neurological diseases, including Alzheimer's disease [66], Parkinson's disease, schizophrenia [67–69], epilepsy, and Charcot-Marie-Tooth disease [70], as well as sense disorders (e.g. anosmia) [71] result from or are linked to defects in TRP function, with affected individuals exhibiting decreased neural plasticity. It has also been shown that TRPV1 could be a target for cognitive decline in Alzheimer's patients. The levels of the TRPV1 agonist anandamide were found to negatively correlate with amyloid-β (Aβ) peptide levels in AD brains [72]. Additionally, application of the TRPV1 agonist capsaicin restores proper gamma oscillations to hippocampal slices that have disrupted gamma oscillations due to over expressed Aβ. The efficacy of capsaicin requires TRPV1 expression as it has no effect on slices from TRPV1 knockout mice [73]. Rat models of biliary cirrhosis, which induces memory impairment, have decreased memory impairment when treated with capsaicin, which also increased TRPV1 and CREB mRNA in the CA1 area of the hippocampus [74]. Recent research even suggests the use of TRPV1 agonists as therapeutics to aid in ameliorating the effects of schizophrenia since TRPV1 is linked to pain and cognitive defects in schizophrenic patients [69]. This could indicate that TRPV1-mediated plasticity defects may underlie some of these neurological disorders. Performing *in vivo* studies to understand how TRPV proteins regulate proper neurological function may uncover a role in learning and memory and could potentially help us to understand what happens in the TRPV1-mediated disease states. We aimed to elucidate how TRP protein functions at the molecular level to promote plasticity and memory formation.

Understanding the molecular mechanisms and dynamics by which animals learn to ignore non-beneficial stimuli through TRP-mediated neural plasticity may be of importance to understanding not only how animals learn and form memories, but may also give insights into the etiology of TRP-mediated neurological diseases.

Materials and methods

Strains and genetics

Strains were maintained by standard methods [75] and were grown on either 5.5 cm or 10 cm Petri dishes with NGM media seeded with OP50 *E. coli*. All strains were grown at and assayed at 20°C. The wild-type strain is the *C. elegans* N2 Bristol variant. Mutants used in the study include *osm-9(ky10) IV* [25]*, osm-9(ok1677) IV, osm-9(yz6) IV*, and SH272 (*osm-9* CRISPR-Cas9 whole-gene deletion strain), a generous gift from Sarah Hall. All rescue experiments (Fig 1, S2 Fig, S4 Fig) were performed in the *osm-9(ky10) IV* background. The transgenic lines used for the rescue experiments are JZ1967 and JZ1968 [*KBC41/*$_p$*odr-3::osm-9::UTR* (50 ng/μl), $_p$*unc-122::mCherry* (20 ng/μl)], (Fig 1); JZ2034, JZ2035, and JZ2036 [*KBC56/*$_p$*osm-9::osm-9::UTR* (50 ng/μl), *pCFJ90/ pmyo-2::mCherry* (2.5 ng/μl), *pSMdelta* (100 ng/μl)], (S2 Fig); JZ1655 and JZ1656 [*KBC8/*$_p$*ceh-36::GFP::osm-9* (100 ng/μl), $_p$*unc-122::GFP* (20 ng/μl)], (S4A Fig); JZ1621 and JZ1622 [*pJK21/*$_p$*odr-3::GFP::osm-9* (50 ng/μl), $_p$*unc-122::mCherry* (20ng/μl), ScaI-digested N2 DNA (30 ng/μl)], (S4B Fig); JZ1819 and JZ1874 [*KBC24/*$_p$*odr-3::osm-9* (50 ng/μl), *pCFJ104/*$_p$*myo-3::mCherry* (5 ng/μl)], (S4C Fig); JZ1940 and JZ1941 [fosmid WRM065bE12 (from Source BioScience, 5 ng/μl), $_p$*unc-122::GFP* (20 ng/μl), $_p$*str-2::GCaMP3::mCherry* (25 ng/μl)], (S4D Fig); lines containing *osm-9::GFP5* (25 ng/

µl), *punc-122::mCherry* (20 ng/µl), (S4E Fig); lines containing *KBC42/ posm-9::osm-9::UTR* (50 ng/µl), *punc-122::mCherry* (20 ng/µl) or *KBC42/ posm-9::osm-9::UTR* (10 ng/µl), *pCFJ90/pmyo-2::mcherry* (2.5 ng/µl), *pSMdelta* (140 ng/µl), (S4F Fig); JZ1905 and JZ1906 [*KBC38/pnphp-4::osm-9::GFP* (5 ng/µl), *punc-122::mCherry* (20 ng/µl); *osm-9(ky10) IV* gDNA (8 ng/µl); *pceh-36::mCherry* (5 ng/µl)], (S4G Fig). ScaI-digested N2 DNA, *osm-9(ky10) IV* gDNA, or *pSMdelta* (empty vector) were used to bring up the total injection concentration to ensure transgenesis [76]. JZ designations are L'Etoile lab strain names. The strain used for cell ID and diacetyl chemotaxis experiments was generated by crossing male *osm-9(py8*) animals with hermaphrodite CA1200 animals. Worms were outcrossed three times with male wild-type N2s. The strain used in NeuroPAL cell ID was created by crossing male otIs670 animals with hermaphrodite *osm-9(py8)*;CA1200 animals.

All transgenic lines were made in the *osm-9(py8)*;CA1200 background. The transgenic lines used for cell ID are *osm-9(py8); CA1200;*[p*ocr-4*::mKate2;p*ofm*-1::GFP (25 ng/µl)], *osm-9(py8);CA1200)*p*osm*-10::mCherry;p*ofm*-1::GFP (25 ng/µl)], *osm-9(py8); CA1200;* p*odr-1*::RFP(10 ng/µl);p*ofm-1*::GFP (25 ng/µl)].

Cell Identification

The animals were imaged after the F2 generation was produced. About 10-15 day 1 adult hermaphrodites were put onto 2% agar pads prepared just before imaging. The transgenic animals were paralyzed with 5 mM tetramisole hydrochloride dissolved in M9 buffer [22 mM KH2PO4, 42 mM Na2HPO4, 85.5 mM NaCl, 1 mM MgSO4]. Next, the

animals were imaged on a spinning disk confocal microscope under a 60x oil objective at 23°C using NIS Elements. Z-stacks were taken concurrently using 488 nm and 561 nm lasers for excitation at 200 ms exposure and 100% power, and were analyzed using FIJI. For NeuroPAL cell ID, 10-15 day 1 adult hermaphrodite *osm-9(py8)*;CA1200;otIs670 animals were placed onto a 2% agar pad and paralyzed using 50mM sodium azide diluted in M9 buffer. The animals were imaged on a spinning disk widefield confocal under a 60x water objective at 20°C using MicroManager. Z-stacks were taken sequentially; first, the mNeptune2.5 fluorophore was imaged with a 561 nm laser and a 700/50 nm emission filter. Next, CyOFP was imaged using a 488 nm laser with a 600/50 nm emission filter. Third, the mTagBFT2 was excited using a 405 nm laser with a 450/50 nm emission filter, and then the TagRFP-T fluorophore was excited using the 561 nm laser with a 600/50 nm filter. Finally, brightfield images were taken, and the GFP channel Z-stacks were taken using the 488 nm laser with a 525/50 nm emission filter. The mNeptune2.5 fluorophore was imaged at 100 ms exposure, and the CyOFP, mTagBFT2, and TagTRP-T fluorophores were imaged at 50 ms exposure. Brightfield was also imaged at 50 ms exposure, and the GFP channel was imaged at 200 ms exposure. All 6 channels were imaged using 20% power. The acquired images were analyzed using FIJI, in accordance with the Hobert Lab's guide "Using NeuroPAL for Neural ID" from Columbia University (77).

Molecular Biology

Constructs were made using standard molecular techniques. All constructs made for this paper are available from Addgene. The construct *pJK21/*

$_p$odr-3::osm-9SS::GFP::osm-9cDNA was made by replacing the *$_p$str-2* promoter in *pJK17/$_p$str-2::osm-9SS::GFP::osm-9cDNA*, digested with NotI and AscI restriction enzymes, with the subcloned *$_p$odr-3* fragment from *pJK15/ $_p$odr-3::osm-9SS::GFP::osm-9cDNA*, using NotI and AscI. *KBC8/ $_p$ceh-36::osm-9SS::GFP::osm-9cDNA* was made by amplifying *$_p$ceh-36* with primers KLB30 (TAACGGCCGGCCTCATCAGCCTACACGTCATC) and KLB31 (ACATAGGCGCGCCCGCAAATGGGCGGAGGGT) to add FseI and AscI sites on and digesting *pAW1/$_p$odr-3::osm-9SS::GFP::osm-9cDNA* with FseI and AscI to remove *$_p$odr-3* and subclone the *$_p$ceh-36* fragment in. *KBC41/$_p$odr-3::osm-9cDNA::UTR* was made by digesting *KBC24/$_p$odr-3::osm-9cDNA* with NheI and NcoI and subcloning in the *osm-9* downstream promoter (~3.2kb), amplified off of phenol-extracted followed by ethanol precipitated whole-worm gDNA (Phenol pH 8 from Sigma Aldrich), using the KLB161 (AGACGCTAGCGAACTTTTTTCTTCTAATTTTTTGA) and KLB162 (AACTCCATGGTTAGGTACATTTAAGGTCGATC) primers, adding on the NheI and NcoI sites. *KBC24/$_p$odr-3::osm-9cDNA* was made by digesting *KBC23/$_p$odr-3* with KpnI and NheI and subcloning in *osm-9* cDNA, amplified from whole-worm cDNA (a kind gift from Maria Gallegos) using primers KLB25 (AACTGGTACCTCATTCGCTTTTGTCATTTGTC) and KLB90 (AGACGCTAGCATGGGCGGTGGAAGTTCG), which add on the KpnI and NheI sites. *KBC42/ $_p$osm-9::osm-9cDNA::UTR* was made by digesting *KBC41/ $_p$odr-3::osm-9cDNA::UTR* with NotI and XmaI and subcloning in the upstream *osm-9* promoter (~1.6 kb), amplified off of phenol-extracted followed by ethanol precipitated whole-worm gDNA (Phenol pH 8 from Sigma Aldrich), using the primers KLB163

(AGACGCGGCCGCCGCGGGAGTACTTTACGGG) and KLB164 (AACTCCCGGGGTTTGGTTTCTGAAAAAATTGG), adding on NotI and XmaI sites. *KBC38/$_p$nphp-4::GFP::osm-9* was made by digesting *KBC26/$_p$odr-3::osm-9cDNA::GFP* with NotI and NruI and subcloning in the *nphp-4* promoter amplified from *pAK59/ $_p$nphp-4::GFP::npp-19* (a kind gift from Piali Sengupta) with primer KLB127 (AGACGCGGCCGCCAACATTATTAATCACTGCAAC) and KLB128 (AACTTCGCGAACTTCCACCGCCCATCTCATTTTTCGAGACTTTGTTA), adding on NotI and NruI sites. KBC56 was made by the following instructions: osm-9 gDNA was amplified with the primers KLB289 (GTTGTTTACCTTTTATGTTCATCCG) and KLB290 (AAATTTTCTACTGCCTGGTATCAAA) off of phenol-extracted followed by ethanol precipitated whole-worm gDNA (Phenol pH 8 from Sigma Aldrich). The *osm-9* gDNA fragment plus extra upstream and downstream homologous sequence was amplified off of the gDNA amplified with KLB289 and KLB290, using the primers KLB298 (GTTGTTTACCTTTTATGTTCAT) and KLB299 (AAAATGATCCACATAAAATTTTCTACTGCCTGGTAT). The *osm-9* upstream partial fragment (~1.2 kb) was amplified using the primers KLB296 (TGATTACGCCAAGCTTCGCGGGAGTACTTTACGG) and KLB297 (TAAAAGGTAAACAACTAGTTTTTAGTACATGAAATAATT) off of the template KBC42/ *$_p$osm-9::osm-9cDNA::UTR*, and the downstream promoter partial fragment was amplified with KLB300 (TATGTGGATCATTTTTGTCTC) and KLB301 (CCGCGCATGCAAGCTTTTAGGTACATTTAAGGTCGAT) off of KBC42/ *$_p$osm-9::osm-9cDNA::UTR*. The three fragments were then recombined in the *pSM*

plasmid (linearized with HindIII) using the Takara Infusion HD Cloning kit. The *pSM* plasmid was from Steve McCarroll.

Short-term memory chemotaxis assay

We utilized the chemotaxis assay from Bargmann et al., 1993 [45]. About 4-5 Larval stage 4 (L4) animals were put onto NGM plates seeded with OP50 *E. coli* for 5 days at 20°C, or until populations are one-day old adults. Any plates with fungal or bacterial contamination were not included in the assays. Animals were then washed off the plates using S. basal buffer and into microfuge tubes (sterile, but not autoclaved), where they were conditioned to either S. basal buffer (0.1M NaCl, 0.05M K_3PO_4, pH 6.0), or 2-butanone (Sigma) diluted in S. basal buffer, 1:10,000 (1.23 mM) concentration. Animals were incubated for 80 minutes on a rotating microfuge tube stand. Next, animals were washed two times with S. basal, where the worms were allowed to pellet (about two to three minutes) without spinning them down. Next, the worms were washed with ddH_2O to ensure all salts were removed, and then placed onto a 10 cm Petri dish chemotaxis plate. The chemotaxis plate media was made by adding 100 mL ddH_2O to 1.6 g of Difco bacto agar, then boiled, and then 500 µl of 1M K_3PO_4, 100 µl 1M $CaCl_2$ and 100 µl 1M $MgSO_4$ were added, and then the media was pipetted at 10 ml per 10 cm plastic petri dish and let cool to solidify, and then square odor arenas and an origin were drawn (S1 Fig). The chemotaxis plate was made with two point sources – one arena with 1 ul of 200-proof ethanol, and the other arena with 1 µl of 1:1000 butanone in ethanol. Each point source also contained 1 µl of 1M sodium azide (Fisher Scientific) to paralyze worms once they reached the arenas (S1 Fig). Animals were placed at the origin, the

liquid was removed with a Kim Wipe, and then animals were allowed to roam for at least two hours. Then, the chemotaxis index or learning index was calculated (Fig 1 legend). For reference, most untrained or buffer-trained wild-type animals have a butanone chemotaxis index from 0.6 to 0.9. If pairwise comparisons between the chemotaxis indices of the buffer-trained and butanone-trained populations of the same genotype were not significantly different from each other, then we deemed them memory defective.

LTM chemotaxis assay

The assay is performed as written above in the “Chemotaxis assay” section, but for three cycles instead of just one, with recovery periods on food in between. Animals are incubated for 80 minutes in either buffer or butanone diluted in buffer. Animals are washed, and then incubated for 30 minutes in OP50 diluted in S. basal buffer (OD = 10). Animals are washed as before, but then conditioned for another 80 minutes in either buffer or diluted butanone, making this the second odor-treatment cycle. Animals are then washed and incubated with OP50 for another 30 minutes, washed, and then subjected to a third buffer or odor conditioning cycle. Animals are then washed as before, and plated onto chemotaxis plates (this is the 0’ recovery, three-cycle trained worms), or recovered on 5.5 cm NGM plates seeded with OP50 for either 30’, 120’, or 16 hours, where they are then subjected to the chemotaxis assay.

WorMotel assay

The WorMotel [55] was used according to previously published methods, as well as this link with more detailed methods (http://fangyenlab.seas.upenn.edu/links.html). In brief, a 48-well PDMS chip called the WorMotel was filled with media and seeded with OP50 (OD = 10), and one worm was placed into each individual well. Behavior was recorded by video using the Multiple Worm Tracker software (https://sourceforge.net/projects/mwt/) and movement was analyzed with Matlab software (KS_analysis_CFY_Jan2019.m and MC_QuiescenceActivity_v1202.fig, both at https://github.com/cfangyen/LEtoile_WorMotel). Excel sheets with total quiescence for each worm is generated from the Matlab code. The mean total quiescence was then taken for statistical analysis.

Statistical Analysis

All data included in the same graph were subjected to the Shapiro-Wilk normality test. If all of the datasets were normally distributed, then one-way ANOVA was performed, followed by Bonferroni correction for pairwise comparisons. If any datasets were non-normally distributed, then the Kruskal-Wallis test was performed. If $p>0.05$, then no further analysis was performed. If $p<0.05$, then the test was followed up by either the Mann-Whitney u-test for non-parametric data pairwise comparisons or the Student's unpaired t-test for parametric data pairwise comparisons. All p-values included in the same graph were then adjusted using the Hochberg test to remove any type I statistical error, which prevents incorrect rejection of the null hypothesis. ***$p<0.001$, **$p<0.01$, *$p<0.05$, NS indicates $p>0.05$. All graphs show S.E.M. Graphpad Prism and R studio were used for all of the statistical tests.

Each data point (represented by grey dots) on the graphs indicates one population of 400>N>50, run on independent days.

Acknowledgements

We would like to thank all past and present members of the L'Etoile lab. We thank Sarah Hall for her gift of the SH272 *osm-9* whole-gene deletion strain, Piali Sengupta for her gift of the *nphp-4* promoter and Cori Bargmann for her gift of the *osm-9::GFP5* construct. We would also like to thank Chris Fang-Yen and Matt Churgin for their help with the WorMotel and the Matlab analysis, and Joe Hill for the artwork used in S1 and S2 Figs. We thank the Caenorhabditis Genetics Center (CGC), supported by the NIH Office of Research Infrastructure Programs (P40 OD010440), for the strains they provided for this study. We are grateful to the team behind wormbase.org (NIH grant #U24 HG002223), SMART (Schultz et al., 1998, EMBL), and Nikhil Bhatla for the wormweb.org exon-intron graphic maker used for Fig 7A.

References

1. Lent CM. Cellular Basis of Behavior. An Introduction to Behavioral Neurobiology. Eric R. Kandel. Q Rev Biol. 1977;52: 326–327. doi:10.1086/410090

2. Fox K, Stryker M. Integrating Hebbian and homeostatic plasticity: introduction. Philos Trans R Soc B. 2017;372. doi:10.1098/rstb.2016.0413

3. Turrigiano G, Leslie KR, Desai NS, Rutherford LC, Nelson SB. Activity-dependent scaling of quantal amplitude in neocortical neurons. Nature. 1998;391: 892–896. doi:10.1038/36103

4. Bailey CH, Kandel ER, Harris KM. Structural Components of Synaptic Plasticity and Memory Consolidation. Cold Spring Harb Perspect Biol. 2015;7: a021758. doi:10.1101/cshperspect.a021758

5. Cosens DJ, Manning A. Abnormal Electroretinogram from a Drosophila Mutant. Nature. 1969;224: 285–287. doi:10.1038/224285a0

6. Montell C, Rubin GM. Molecular characterization of the drosophila trp locus: A putative integral membrane protein required for phototransduction. Neuron. 1989;2: 1313–1323. doi:10.1016/0896-6273(89)90069-X

7. Minke B. The History of the *Drosophila* TRP Channel: The Birth of a New Channel Superfamily. J Neurogenet. 2010;24: 216–233. doi:10.3109/01677063.2010.514369

8. Wang Y, editor. Transient Receptor Potential Canonical Channels and Brain Diseases [Internet]. Dordrecht: Springer Netherlands; 2017. doi:10.1007/978-94-024-1088-4

9. Muller C, Morales P, Reggio PH. Cannabinoid Ligands Targeting TRP Channels. Front Mol Neurosci. 2019;11: 487. doi:10.3389/fnmol.2018.00487

10. De Petrocellis L, Ligresti A, Moriello AS, Allarà M, Bisogno T, Petrosino S, et al. Effects of cannabinoids and cannabinoid-enriched Cannabis extracts on TRP channels and endocannabinoid metabolic enzymes: Novel pharmacology of minor plant cannabinoids. Br J Pharmacol. 2011;163: 1479–1494. doi:10.1111/j.1476-5381.2010.01166.x

11. De Petrocellis L, Nabissi M, Santoni G, Ligresti A. Actions and Regulation of Ionotropic Cannabinoid Receptors. Advances in Pharmacology. Elsevier; 2017. pp. 249–289. doi:10.1016/bs.apha.2017.04.001

12. Hellmich UA, Gaudet R. Structural Biology of TRP Channels. In: Nilius B, Flockerzi V, editors. Mammalian Transient Receptor Potential (TRP) Cation Channels. Cham: Springer International Publishing; 2014. pp. 963–990. doi:10.1007/978-3-319-05161-1_10

13. Julius D. TRP channels and pain. Annu Rev Cell Dev Biol. 2013;29: 355—384. doi:10.1146/annurev-cellbio-101011-155833

14. Sawamura S, Shirakawa H, Nakagawa T, Mori Y, Kaneko S. TRP Channels in the Brain. 2017. pp. 295–322. doi:10.4324/9781315152837-16

15. Eguchi N, Hishimoto A, Sora I, Mori M. Slow synaptic transmission mediated by TRPV1 channels in CA3 interneurons of the hippocampus. Neurosci Lett. 2016;616: 170–176. doi:10.1016/j.neulet.2015.12.065

16. Marsch R, Foeller E, Rammes G, Bunck M, Kossl M, Holsboer F, et al. Reduced Anxiety, Conditioned Fear, and Hippocampal Long-Term Potentiation in Transient Receptor Potential Vanilloid Type 1 Receptor-Deficient Mice. J Neurosci. 2007;27: 832–839. doi:10.1523/JNEUROSCI.3303-06.2007

17. Gibson HE, Edwards JG, Page RS, Van Hook MJ, Kauer JA. TRPV1 Channels Mediate Long-Term Depression at Synapses on Hippocampal Interneurons. Neuron. 2008;57: 746–759. doi:10.1016/j.neuron.2007.12.027

18. Sakai T, Sato S, Ishimoto H, Kitamoto T. Significance of the centrally expressed TRP channel painless in Drosophila courtship memory. Learn Mem. 2012;20: 34–40. doi:10.1101/lm.029041.112

19. Abramowitz J, Yildirim E, Birnbaumer L. The TRPC Family of Ion Channels: Relation to the TRP Superfamily and Role in Receptor- and Store-Operated Calcium Entry. In: Liedtke WB, Heller S, editors. TRP Ion Channel Function in Sensory Transduction and Cellular Signaling Cascades. Boca Raton (FL): CRC Press/Taylor & Francis; 2007.

20. Tai Y, Feng S, Ge R, Du W, Zhang X, He Z, et al. TRPC6 channels promote dendritic growth via the CaMKIV-CREB pathway. J Cell Sci. 2008;121: 2301—2307. doi:10.1242/jcs.026906

21. Zhou J, Du W, Zhou K, Tai Y, Yao H, Jia Y, et al. Critical role of TRPC6 channels in the formation of excitatory synapses. Nat Neurosci. 2008;11: 741—743. doi:10.1038/nn.2127

22. Bovet-Carmona M, Menigoz A, Pinto S, Tambuyzer T, Krautwald K, Voets T, et al. Disentangling the role of TRPM4 in hippocampus-dependent plasticity and learning: an electrophysiological, behavioral and FMRI approach. Brain Struct Funct. 2018;223: 3557–3576. doi:10.1007/s00429-018-1706-1

23. Genro BP, de Oliveira Alvares L, Quillfeldt JA. Role of TRPV1 in consolidation of fear memories depends on the averseness of the conditioning procedure. Neurobiol Learn Mem. 2012;97: 355–360. doi:10.1016/j.nlm.2012.01.002

24. Li H-B, Mao R-R, Zhang J-C, Yang Y, Cao J, Xu L. Antistress Effect of TRPV1 Channel on Synaptic Plasticity and Spatial Memory. Biol Psychiatry. 2008;64: 286–292. doi:10.1016/j.biopsych.2008.02.020

25. Colbert H, Bargmann CI. Odorant-specific adaptation pathways generate olfactory plasticity in C. elegans. Neuron. 1995;14: 803–812.

26. Kaufmann AL, Ashraf JM, Corces-Zimmerman R, Landis JN, Murphy CT. Insulin Signaling and Dietary Restriction Differentially Influence the Decline of Learning and Memory with Age. PLOS Biol. 2010;8: e1000372. doi:10.1371/journal.pbio.1000372

27. Muñoz-Lobato F, Chanrda, R. Benedetti KL, Farah F, Saifuddin, F, A, MNordquist SK, Bokka A, Brueggemann C, et al. Sleep is required to remodel specific synapses for memory consolidation. BioRxiv 2020.11.24.395228; doi: https://doi.org/ 10.1101/2020.11.24.395228.

28. White JG, Southgate E, Thomson JN, Brenner S. The structure of the nervous system of the nematode C. elegans. Philos Trans R Soc B. 1986;314: 1–340.

29. Cook SJ, Jarrell TA, Brittin CA, Wang Y, Bloniarz AE, Yakovlev MA, et al. Whole-animal connectomes of both Caenorhabditis elegans sexes. Nature. 2019;571: 63–71. doi:10.1038/s41586-019-1352-7

30. Kaiser M. Neuroanatomy: Connectome Connects Fly and Mammalian Brain Networks. Curr Biol. 2015;25: R416–R418. doi:10.1016/j.cub.2015.03.039

31. Cho CE, Brueggemann C, L'Etoile ND, Bargmann CI. Parallel encoding of sensory history and behavioral preference during Caenorhabditis elegans olfactory learning. eLife. 2016;5: e14000. doi:10.7554/eLife.14000

32. Gordus A, Pokala N, Levy S, Flavell SW, Bargmann CI. Feedback from network states generates variability in a probabilistic olfactory circuit. Cell. 2015;161: 215–227. doi:10.1016/j.cell.2015.02.018

33. Vennekens R, Hoenderop JGJ, Prenen J, Stuiver M, Willems PHGM, Droogmans G, et al. Permeation and Gating Properties of the Novel Epithelial Ca $^{2+}$ Channel. J Biol Chem. 2000;275: 3963–3969. doi:10.1074/jbc.275.6.3963

34. Nilius B, Vennekens R, Prenen J, Hoenderop JG, Bindels RJ, Droogmans G. Whole-cell and single channel monovalent cation currents through the novel rabbit epithelial Ca2+ channel ECaC. J Physiol. 2000;527 Pt 2: 239–248. doi:10.1111/j.1469-7793.2000.00239.x

35. Dang S, van Goor MK, Asarnow D, Wang Y, Julius D, Cheng Y, et al. Structural insight into TRPV5 channel function and modulation. Proc Natl Acad Sci. 2019;116: 8869–8878. doi:10.1073/pnas.1820323116

36. van Goor MKC, Hoenderop JGJ, van der Wijst J. TRP channels in calcium homeostasis: from hormonal control to structure-function relationship of TRPV5 and TRPV6. Biochim Biophys Acta BBA - Mol Cell Res. 2017;1864: 883–893. doi:10.1016/j.bbamcr.2016.11.027

37. Colbert HA, Smith TL, Bargmann CI. OSM-9, A Novel Protein with Structural Similarity to Channels, Is Required for Olfaction, Mechanosensation, and Olfactory Adaptation in *Caenorhabditis elegans*. J Neurosci. 1997;17: 8259–8269. doi:10.1523/JNEUROSCI.17-21-08259.1997

38. Tobin DM, Madsen DM, Kahn-Kirby A, Peckol EL, Moulder G, Barstead R, et al. Combinatorial Expression of TRPV Channel Proteins Defines Their Sensory Functions

and Subcellular Localization in C. elegans Neurons. Neuron. 2002;35: 307–318. doi:10.1016/S0896-6273(02)00757-2

39. Lindy AS, Parekh PK, Zhu R, Kanju P, Chintapalli SV, Tsvilovskyy V, et al. TRPV channel-mediated calcium transients in nociceptor neurons are dispensable for avoidance behaviour. Nat Commun. 2014;5: 4734. doi:10.1038/ncomms5734

40. Kahn-Kirby AH, Dantzker JLM, Apicella AJ, Schafer WR, Browse J, Bargmann CI, et al. Specific Polyunsaturated Fatty Acids Drive TRPV-Dependent Sensory Signaling In Vivo. Cell. 2004;119: 889–900. doi:10.1016/j.cell.2004.11.005

41. Upadhyay A, Pisupati A, Jegla T, Crook M, Mickolajczyk KJ, Shorey M, et al. Nicotinamide is an endogenous agonist for a C. elegans TRPV OSM-9 and OCR-4 channel. Nat Commun. 2016;7: 13135. doi:10.1038/ncomms13135

42. Hall SE, Beverly M, Russ C, Nusbaum C, Sengupta P. A Cellular Memory of Developmental History Generates Phenotypic Diversity in C. elegans. Curr Biol. 2010;20: 149–155. doi:10.1016/j.cub.2009.11.035

43. Sims JR, Ow MC, Nishiguchi MA, Kim K, Sengupta P, Hall SE. Developmental programming modulates olfactory behavior in C. elegans via endogenous RNAi pathways. eLife. 2016;5: e11642. doi:10.7554/eLife.11642

44. Bargmann CI, Horvitz HR. Chemosensory neurons with overlapping functions direct chemotaxis to multiple chemicals in C. elegans. Neuron. 1991;7: 729–742. doi:https://doi.org/10.1016/0896-6273(91)90276-6

45. Bargmann CI, Hartweig E, Horvitz HR. Odorant-selective genes and neurons mediate olfaction in C. elegans. Cell. 1993;74: 515–527. doi:10.1016/0092-8674(93)80053-h

46. L'Etoile ND, Bargmann CI. Olfaction and Odor Discrimination Are Mediated by the C. elegans Guanylyl Cyclase ODR-1. Neuron. 2000;25: 575–586. doi:10.1016/S0896-6273(00)81061-2

47. Birnby DA, Link EM, Vowels JJ, Tian H, Colacurcio PL, Thomas JH. A Transmembrane Guanylyl Cyclase (DAF-11) and Hsp90 (DAF-21) Regulate a Common Set of Chemosensory Behaviors in Caenorhabditis elegans. Genetics. 2000;155: 85–104.

48. L'Etoile ND, Coburn CM, Eastham J, Kistler A, Gallegos G, Bargmann CI. The Cyclic GMP-Dependent Protein Kinase EGL-4 Regulates Olfactory Adaptation in C. elegans. Neuron. 2002;36: 1079–1089. doi:10.1016/S0896-6273(02)01066-8

49. O'Halloran DM, Altshuler-Keylin S, Lee JI, L'Etoile ND. Regulators of AWC-Mediated Olfactory Plasticity in Caenorhabditis elegans. Chisholm AD, editor. PLoS Genet. 2009;5: e1000761. doi:10.1371/journal.pgen.1000761

50. Lee JI, O'Halloran DM, Eastham-Anderson J, Juang B-T, Kaye JA, Scott Hamilton O, et al. Nuclear entry of a cGMP-dependent kinase converts transient into long-lasting olfactory adaptation. Proc Natl Acad Sci. 2010;107: 6016–6021. doi:10.1073/pnas.1000866107

51. Juang B-T, Gu C, Starnes L, Palladino F, Goga A, Kennedy S, et al. Endogenous Nuclear RNAi Mediates Behavioral Adaptation to Odor. Cell. 2013;154: 1010–1022. doi:10.1016/j.cell.2013.08.006

52. Lakhina V, Arey RN, Kaletsky R, Kauffman A, Stein G, Keyes W, et al. Genome-wide Functional Analysis of CREB/Long-Term Memory-Dependent Transcription

Reveals Distinct Basal and Memory Gene Expression Programs. Neuron. 2015;85: 330–345. doi:10.1016/j.neuron.2014.12.029

53. Dudai Y. Consolidation: Fragility on the Road to the Engram. Neuron. 1996;17: 367–370. doi:10.1016/S0896-6273(00)80168-3

54. Dudai Y. The Neurobiology of Consolidations, Or, How Stable is the Engram? Annu Rev Psychol. 2004;55: 51–86. doi:10.1146/annurev.psych.55.090902.142050

55. Churgin MA, Jung S-K, Yu C-C, Chen X, Raizen DM, Fang-Yen C. Longitudinal imaging of Caenorhabditis elegans in a microfabricated device reveals variation in behavioral decline during aging. eLife. 2017;6: e26652. doi:10.7554/eLife.26652

56. Ruggiero RN, Rossignoli MT, De Ross JB, Hallak JEC, Leite JP, Bueno-Junior LS. Cannabinoids and Vanilloids in Schizophrenia: Neurophysiological Evidence and Directions for Basic Research. Front Pharmacol. 2017;8: 399. doi:10.3389/fphar.2017.00399

57. Grueter BA, Brasnjo G, Malenka RC. Postsynaptic TRPV1 triggers cell type–specific long-term depression in the nucleus accumbens. Nat Neurosci. 2010;13: 1519–1525. doi:10.1038/nn.2685

58. Lovelace JW, Vieira PA, Corches A, Mackie K, Korzus E. Impaired Fear Memory Specificity Associated with Deficient Endocannabinoid-Dependent Long-Term Plasticity. Neuropsychopharmacology. 2014;39: 1685–1693. doi:10.1038/npp.2014.15

59. Hammarlund M, Hobert O, Miller DM, Sestan N. The CeNGEN Project: The Complete Gene Expression Map of an Entire Nervous System. Neuron. 2018;99: 430–433. doi:10.1016/j.neuron.2018.07.042

60. Peng G, Shi X, Kadowaki T. Evolution of TRP channels inferred by their classification in diverse animal species. Mol Phylogenet Evol. 2015;84: 145–157. doi:10.1016/j.ympev.2014.06.016

61. Kang K, Pulver SR, Panzano VC, Chang EC, Griffith LC, Theobald DL, et al. Analysis of Drosophila TRPA1 reveals an ancient origin for human chemical nociception. Nature. 2010;464: 597–600. doi:10.1038/nature08848

62. Wang DY-C, Kumar S, Hedges SB. Divergence time estimates for the early history of animal phyla and the origin of plants, animals and fungi. Proc R Soc Lond B Biol Sci. 1999;266: 163–171. doi:10.1098/rspb.1999.0617

63. Chen J, Zhang X-F, Kort ME, Huth JR, Sun C, Miesbauer LJ, et al. Molecular Determinants of Species-Specific Activation or Blockade of TRPA1 Channels. J Neurosci. 2008;28: 5063–5071. doi:10.1523/JNEUROSCI.0047-08.2008

64. Xiao B, Dubin AE, Bursulaya B, Viswanath V, Jegla TJ, Patapoutian A. Identification of Transmembrane Domain 5 as a Critical Molecular Determinant of Menthol Sensitivity in Mammalian TRPA1 Channels. J Neurosci. 2008;28: 9640–9651. doi:10.1523/JNEUROSCI.2772-08.2008

65. Nagatomo K, Ishii H, Yamamoto T, Nakajo K, Kubo Y. The Met268Pro Mutation of Mouse TRPA1 Changes the Effect of Caffeine from Activation to Suppression. Biophys J. 2010;99: 3609–3618. doi:10.1016/j.bpj.2010.10.014

66. Di Marzo V, Gobbi G, Szallasi A. Brain TRPV1: a depressing TR(i)P down memory lane? Trends Pharmacol Sci. 2008;29: 594–600. doi:10.1016/j.tips.2008.09.004

67. Tzavara ET, Li DL, Moutsimilli L, Bisogno T, Di Marzo V, Phebus LA, et al. Endocannabinoids Activate Transient Receptor Potential Vanilloid 1 Receptors to

Reduce Hyperdopaminergia-Related Hyperactivity: Therapeutic Implications. Biol Psychiatry. 2006;59: 508–515. doi:10.1016/j.biopsych.2005.08.019

68. Almeida V, Peres FF, Levin R, Suiama MA, Calzavara MB, Zuardi AW, et al. Effects of cannabinoid and vanilloid drugs on positive and negative-like symptoms on an animal model of schizophrenia: The SHR strain. Schizophr Res. 2014;153: 150–159. doi:10.1016/j.schres.2014.01.039

69. Madasu MK, Roche M, Finn DP. Supraspinal Transient Receptor Potential Subfamily V Member 1 (TRPV1) in Pain and Psychiatric Disorders. In: Finn DP, Leonard BE, editors. Modern Trends in Pharmacopsychiatry. S. Karger AG; 2015. pp. 80–93. doi:10.1159/000435934

70. Morelli MB, Amantini C, Liberati S, Santoni M, Nabissi M. TRP Channels: New Potential Therapeutic Approaches in CNS Neuropathies. Former Curr Drug Targets - CNS Neurol Disord. 2013;12: 274–293. doi:10.2174/18715273113129990056

71. Nilius B. TRP channels in disease. Biochim Biophys Acta BBA - Mol Basis Dis. 2007;1772: 805–812. doi:10.1016/j.bbadis.2007.02.002

72. Jung K-M, Astarita G, Yasar S, Vasilevko V, Cribbs DH, Head E, et al. An amyloid β42-dependent deficit in anandamide mobilization is associated with cognitive dysfunction in Alzheimer's disease. Neurobiol Aging. 2012;33: 1522–1532. doi:10.1016/j.neurobiolaging.2011.03.012

73. Balleza-Tapia H, Crux S, Andrade-Talavera Y, Dolz-Gaiton P, Papadia D, Chen G, et al. TrpV1 receptor activation rescues neuronal function and network gamma oscillations from Ab-induced impairment in mouse hippocampus in vitro. : 24. doi:10.7554/eLife.37703

74. Bashiri H, Hosseini-Chegeni H, Alsadat Sharifi K, Sahebgharani M, Salari A-A. Activation of TRPV1 receptors affects memory function and hippocampal TRPV1 and CREB mRNA expression in a rat model of biliary cirrhosis. Neurol Res. 2018;40: 938–947. doi:10.1080/01616412.2018.1504158

75. Brenner S. The genetics of Caenorhabditis elegans. Genetics. 1974;77: 71–94.

76. Evans T. Transformation and microinjection. WormBook. 2006; doi:10.1895/wormbook.1.108.1

77. Yemini, E, Lin, A, Nejatbakhsh, A, Varol, E, Sun, R, Mena, GE, Samuel, ADT, Paninski, L, Venkatachalam, V and Hobert, O "NeuroPAL: A Neuronal Polychromatic Atlas of Landmarks for Whole-Brain Imaging in *C. elegans*", BioRxiv **doi:** https://doi.org/10.1101/676312

Figure Legends

Fig 1. *osm-9* is required for short-term memory, but not memory acquisition post spaced training. (A) Chemotaxis indices for one-cycle odor conditioned and three-cycle odor wild-type vs *osm-9(ky10)* spaced-trained animals. The chemotaxis index (CI) is calculated as the number of worms at the diluent (200-proof ethanol) subtracted from the number at the butanone point source, divided by the total number or worms (excluding any at the origin). Wild-type one- or three-cycle buffer trained (CTL, grey bar), wild-type one- or three-cycle butanone-trained (BTN, red bar), *osm-9(ky10)* one- or three-cycle buffer-trained (CTL, pink bar) and *osm-9(ky10)* one- or three-cycle butanone-trained (BTN, purple bar) are shown, and are denoted this way throughout the rest of the manuscript. "Three-cycle trained" label means 0' recovery (fifth to eighth bars) and will be annotated this way throughout the paper. N = number of trials where all

trials are done on independent days and each grey dot represents an individual assay day, with 50-200 animals/day. The Shapiro-Wilk normality test was performed to determine data distribution, and if data were non-normally distributed, the analysis was done with the Kruskal-Wallis test, an analysis of variance of multiple comparisons for non-parametric data. If pairwise comparisons were normally distributed, then p-values were generated with a Student's unpaired t-test. If any of the datasets were non-parametric, then p-values were generated with the Mann-Whitney u-test. Hochberg adjustment for multiple comparisons was performed on all p-values generated from data included in the same graph to control Type I statistical error. If the data were normally distributed, then one-way ANOVA was performed, followed by Bonferroni correction of pairwise comparisons. Error bars represent S.E.M. Statistical significance was reported as ***p<0.001, ** p< 0.01, *p<0.05, and NS is p>0.05. Behavioral data throughout the paper are represented in this same way with the same numbers of animals on independent days. Additionally, throughout the paper, the same statistical analysis was performed on the data. Note that for every figure in this manuscript, that the Kruskal-Wallis or one-way ANOVA test was performed and yielded ***p<0.001, unless otherwise noted. The Kruskal-Wallis test was performed. The u-test was performed for one-cycle CTL vs BTN, one-cycle *osm-9(ky10)* CTL vs *osm-9(ky10)* BTN, three-cycle trained *osm-9(ky10)* CTL vs *osm-9(ky10)* BTN, one-cycle *osm-9(ky10)* BTN vs three-cycle *osm-9(ky10)* BTN, and three-cycle BTN vs *osm-9(ky10)* BTN. The t-test was performed for one-cycle BTN vs *osm-9(ky10)* BTN, three-cycle CTL vs BTN, and one-cycle BTN vs three-cycle BTN.

(B) Learning indices for one-cycle conditioned and three-cycle spaced-trained wild-type vs *osm-9(ky10)* animals. The learning index (LI) is calculated as the chemotaxis index of the BTN animals subtracted from the chemotaxis index of the CTL animals. The higher the learning index, the more the animals have learned and thus kept the BTN memory. Wild type is shown with grey bars and *osm-9(ky10)* with pink bars, and will be denoted this way throughout the manuscript. One-way ANOVA followed by Bonferroni correction was performed for one-cycle wild type vs *osm-9(ky10)*, one-cycle vs three-cycle wild type, one-cycle wild type vs three-cycle *osm-9(ky10),* one-cycle *osm-9(ky10)* vs three-cycle wild type, one-cycle vs three-cycle *osm-9(ky10)*, and three-cycle wild type vs *osm-9(ky10).*

Fig 2. *osm-9* is required for long-term olfactory memory consolidation post spaced training. (A) Chemotaxis indices for three-cycle spaced-trained animals after 0', 30' or 120' post recovery on plates seeded with OP50 as a food source. One-way ANOVA followed by Bonferroni correction was performed for CTL vs BTN, *osm-9(ky10)* CTL vs *osm-9(ky10)* BTN, CTL 30' vs BTN 30', *osm-9(ky10)* CTL 30' vs *osm-9(ky10)* BTN 30', CTL 120' vs BTN 120', *osm-9(ky10)* CTL 120' vs *osm-9(ky10)* BTN 120', CTL vs *osm-9(ky10)* CTL, BTN vs *osm-9(ky10)* BTN, CTL 30' vs *osm-9(ky10)* CTL 30', BTN 30' vs *osm-9(ky10)* BTN 30', CTL 120' vs *osm-9(ky10)* CTL 120', BTN 120' vs *osm-9(ky10)* BTN 120', BTN vs BTN 30', *osm-9(ky10)* BTN vs *osm-9(ky10)* BTN 30', BTN 30' vs BTN 120', and *osm-9(ky10)* BTN 30' vs *osm-9(ky10)* BTN 120'.

(B) Learning indices for three-cycle spaced-trained animals after 0', 30', or 120' recovery on food. One-way ANOVA followed by Bonferroni correction was performed for

wild-type vs *osm-9(ky10)* after 0' recovery (compare first two bars), 30' recovery (compare third and fourth bars), 120' recovery (compare fifth and sixth bars), wild-type 0' vs 30' *osm-9(ky10)* 0' vs 30', *osm-9(ky10)* 30' vs 120', wild-type 0' vs 120', *osm-9(ky10)* 0' vs 120', and wild-type 30' vs 120', all after three-cycle spaced-training.

Fig 3. *osm-9* animals do not maintain the memory 16 hours after training. (A) Chemotaxis indices for three-cycle trained animals after 0' vs 16 hours of recovery on food. The Kruskal-Wallis test was performed. The u-test was performed for *osm-9(ky10)* CTL vs *osm-9(ky10)* BTN, CTL 16 hr vs BTN 16 hr, *osm-9(ky10)* BTN vs *osm-9(ky10)* BTN 16hr, and BTN vs *osm-9(ky10)* BTN. The t-test was performed for CTL vs BTN, BTN 16 hr vs *osm-9(ky10)* BTN 16 hr, *osm-9(ky10)* CTL 16 hr vs *osm-9(ky10)* BTN 16 hr, and BTN vs BTN 16 hr.

(B) Learning indices for three-cycle trained animals after 0' vs 16 hours of recovery on food. The Kruskal-Wallis test was performed. The u-test was performed for wild type 16 hr vs *osm-9(ky10)* 16 hr, wild type 0' vs wild type 16 hr, and *osm-9(ky10)* 0' vs wild type 16 hr. The t-test was performed for wild type 0' vs *osm-9(ky10)* 0', *osm-9(ky10)* 0' vs *osm-9(ky10)* 16 hr, and wild type 0' vs *osm-9(ky10)* 16 hr.

Fig 4. Spaced-training does not induce a difference in quiescence between wild type and *osm-9(ky10)*. (A) Raster plot of activity of wild-type and *osm-9(ky10)* animals 15-75 minutes after three-cycle spaced training. Animals were placed in a WorMotel [55]

and videos were taken of their movement. Worm number is shown on the y-axis where each row represents one worm, with 24 worms total shown per plot. Yellow indicates activity and blue indicates quiescence, which was defined as no movement for more than 30 seconds.

(B) The mean total quiescence after spaced training is not significantly different between wild-type and *osm-9(ky10)* animals. Mean total quiescence in minutes per hour of animals in a WorMotel. Each grey dot represents 24 animals tested per condition on an independent day. The t-test was performed.

Fig 5. The *osm-9(ok1677), osm-9(yz6)*, and *osm-9* (whole gene-deletion) animals also can acquire, but cannot maintain long-term memory. (A) Gene map of *osm-9.* Exons are denoted by black boxes and introns are black lines connecting the exons. Red-violet indicates ankyrin repeats (six total). Orange indicates a PKD channel domain. The 5' end white box represents an ~1.6 kb promoter region [37]. The 3' end white box represents an ~3.2 kb promoter region [37]. Scale bar indicates 1000 bases. Black arrowheads indicate alleles with point mutations producing early stop codons (*ky10* and *yz6*). The bracket labeled *ok1677* denotes a deletion allele. The brackets labeled ncRNA and tRNA are predicted RNAs produced from these regions. The bracket labeled pore loop denotes the region permeable to calcium, located between the fifth and sixth transmembrane domains.

(B) Chemotaxis indices for three-cycle trained animals with no recovery or 16 hours recovery on food for wild-type, *osm-9(ok1677)*, *osm-9(yz6)*, and *osm-9 (deletion,* which

is a whole-gene deletion) animals. Grey and red bars are wild-type buffer- and butanone-trained animals and pink and purple are *osm-9* buffer- and butanone-trained animals. One-way ANOVA, followed by Bonferroni correction was performed for three-cycle CTL vs BTN, three-cycle *osm-9(ok1677)* CTL vs *osm-9(ok1677)* BTN, three-cycle *osm-9(yz6)* CTL vs *osm-9(yz6)* BTN, three-cycle *osm-9*(deletion) CTL vs *osm-9*(deletion) BTN, 16 hr CTL vs BTN, 16 hr *osm-9(ok1677)* CTL vs *osm-9(ok1677)* BTN, 16 hr *osm-9(yz6)* CTL vs *osm-9(yz6)* BTN, 16 hr *osm-9*(deletion) CTL vs 16 hr *osm-9*(deletion) BTN, three-cycle BTN vs three-cycle *osm-9(ok1677)* BTN, three-cycle *osm-9(ok1677)* BTN vs three-cycle *osm-9(yz6)* BTN, three-cycle *osm-9(yz6)* BTN vs three-cycle *osm-9*(deletion), 16 hr BTN vs 16 hr *osm-9(ok1677)* BTN, 16 hr *osm-9(ok1677)* BTN vs 16 hr *osm-9(yz6)* BTN, 16 hr *osm-9(yz6)* BTN vs 16 hr *osm-9*(deletion), three-cycle BTN vs 16 hr BTN, three-cycle *osm-9(ok1677)* BTN vs 16 hr *osm-9(ok1677)* BTN, three-cycle *osm-9(yz6)* BTN vs 16 hr *osm-9(yz6)* BTN, and three-cycle *osm-9*(deletion) BTN vs 16 hr *osm-9*(deletion) BTN.

Fig 6. Expressing *osm-9* cDNA under the endogenous and OSN promoters in *ky10* partially rescues short-term memory. (A) Chemotaxis indices of one-cycle trained animals. Chemotaxis indices of one 80-minute cycle buffer (CTL, first bar, grey) vs butanone-trained (BTN, second bar, red) wild-type animals, buffer-trained (CTL, third bar, teal) vs butanone-trained (BTN, fourth bar, light blue) *osm-9(ky10) IV;* $_p$*OSN::osm-9* animals, and buffer-trained (CTL, fifth bar, pink) vs butanone-trained (BTN, sixth bar, purple) non-transgenic siblings. The transgene is *KBC41/*$_p$*OSN::osm-9::UTR.* The $_p$*OSN* is the $_p$*odr-3* olfactory sensory neuron promoter, driving expression in the AWA, AWB,

and AWC neurons, *osm-9* is the full length cDNA (~2.8 kb), and is also driven by the 3' UTR downstream endogenous promoter (~3.2 kb) shown to drive expression in various sensory neurons [37]. Transgenic data is from two combined lines. For Fig 1A, one-way ANOVA was performed, followed by the Bonferroni correction for multiple comparisons for CTL vs BTN, CTL vs BTN *osm-9(ky10); +$_p$OSN::osm-9*, CTL vs BTN *osm-9(ky10); -$_p$OSN::osm-9* (non-transgenic siblings), CTL *osm-9(ky10); +$_p$OSN::osm-9* vs CTL *osm-9(ky10); -$_p$OSN::osm-9*, BTN *osm-9(ky10); +$_p$OSN::osm-9* vs CTL *osm-9(ky10); -$_p$OSN::osm-9*, and BTN *osm-9(ky10); +$_p$OSN::osm-9* vs BTN *osm-9(ky10); -$_p$OSN::osm-9.*

(B) Learning indices for the odor-conditioned animals. One-way ANOVA followed by Bonferroni correction for wild type (first bar, grey) vs *osm-9(ky10); +$_p$OSN::osm-9* (second bar, teal), *osm-9(ky10); +$_p$OSN::osm-9* vs *osm-9(ky10); -$_p$OSN::osm-9* (third bar, pink), and wild type vs *osm-9(ky10); -$_p$OSN::osm-9*.

Fig 7: Degradation of endogenous OSM-9 tagged with and auxin inducible degron phenocopies *osm-9(ky10)* diactetyl chemotaxis defects. A) Auxin-inducible degron tagged OSM-9. The endogenous copy of the *osm-9* gene was edited using CRIPSR to encode a fusion between OSM-9 and at its C-terminus, GFP followed by the auxin inducible degradation signal AID. This is designated *osm-9(py8)*. TIR1 is the substrate recognition component of the he auxin inducible E3 ligase and it is expressed from the ubiquitous promoter *eft-3.* Once TIR1 binds auxin, it induces degradation of target proteins that contain the AID. **B) Auxin induced degradation of OSM-9::GFP::AID phenocopies *osm-9(ky10)* chemotaxis defects to diacetyl.**

Chemotaxis indices for wild type, *osm-9(ky10)* and osm-9(py8); p*eft-3*:: TIR1::GFP::AID to the attractant, (1:1,000) dactyl. Wild type (wt), *osm-9(ky10)* and *osm-9(py8); peft-3:: TIR1::GFP::AID* were exposed to buffer plus 0, 1 mM, 5mM, 10 mM, or 50 mM auxin for 0', 30' 60' or 120' before being subjected to a dactyl chemotaxis assay. One-way ANOVA followed by Bonferroni correction was performed for each comparison shown.

Fig 8: Endogenous Expression of OSM-9 A) Schematic of *C. elegans,* boxes indicate regions imaged: whole head, cilia and phasmids. B) Visualization of endogenous GFP-tagged OSM-9 expression in the *osm-9(py8)* strain in the head, cell bodies are marked with arrows; in the cilia, the AWA cilia with its characteristic morphology expressed GFP and in the tail region, the phasmids PHA/PHB also express GFP. **C) p*odr-1::*RFP marks AWC and AWB in the *osm-9(py8)* strain.** No over lap is seen. **D)p*ocr-4*::mKate2 marks the OLQ neurons in the *osm-9(py8)* strain E) p*osm-10*::mKate2 marks ASH, and ASI neurons in the *osm-9(py8)* strain**. There is overlap between mKate2 and GFP in ASH but not ASI. In panels C-E, markers were expressed in *osm-9(py8)* without p*eft-3*::TIR1::mRuby. **F) Summary of endogenous OSM-9 (*osm-9(py8))* expression.** [1]CenGen data (https://cengen.shinyapps.io/SCeNGEA/). [2]NeuroPal (Yemeni et al., BioRxiv 2019).

Supporting information

S1 Fig. Schematic of one-cycle odor-conditioning. Animals are conditioned to butanone as previously published [51]. In brief, age-synchronized, one-day old adult

animals are washed with buffer from NGM plates containing OP50 food to tubes with either buffer or butanone, both containing no food, for 80 minutes. After the 80-minute incubation, animals are washed and then plated onto chemotaxis assay plates. The chemotaxis index (See Fig 1 legend) is then calculated after at least two hours of the animals roaming.

S2 Fig. Spaced-training paradigm. Schematic of associative olfactory memory assay to induce long-term odor memory. Age-synchronized, one-day old adult animals are washed from plates with food into tubes and are conditioned to either buffer (CTL) or butanone (BTN) for 80 minutes per cycle in the absence of food for three cycles total, with a 30-minute recovery on food (OP50, OD = 10) in between cycles. After spaced-training, animals are either tested in a butanone chemotaxis assay or are recovered on OP50-seeded NGM plates and then tested.

S3 Fig. The *osm-9(yz6)* and *osm-9* (whole gene-deletion) animals cannot chemotax to diacetyl like wild-type and *osm-9(ok1677)* animals. A) Diacetyl chemotaxis indices for wild-type vs *osm-9(ok1677)*, *osm-9(yz6)* and *osm-9* (deletion, which is a whole gene-deletion) animals. Diacetyl chemotaxis assay was performed the same as in the butanone chemotaxis assay, and the diacetyl odor point source was also diluted 1:1000. Wild-type is represented by a grey bar and the *osm-9* alleles are represented by pink bars. One-way ANOVA was performed, followed by Bonferroni correction of wild type vs *osm-9(ok1677)*, wild type vs *osm-9(yz6)*, wild type vs *osm-9*

(deletion), *osm-9(ok1677)* vs *osm-9(yz6)*, *osm-9(ok1677)* vs *osm-9* (deletion), and *osm-9(yz6)* vs *osm-9* (deletion).

S4 Fig. Various *osm-9* expression transgenes are not sufficient to rescue *osm-9(ky10)* one-cycle butanone conditioning defects. (A) Chemotaxis indices of wild type versus *osm-9(ky10),* with or without the transgene *KBC8/ $_p$ceh-36::osm-9SS::GFP::osm-9.* The *pceh-36* is a promoter driving expression in both of the AWC olfactory sensory neurons. The *osm-9SS* (signal sequence) cDNA was 5' of the GFP and the rest of the cDNA was 3' of the GFP. Data shown from six combined transgenic lines. The Kruskal-Wallis test was performed. Transgenic is tg and non-transgenic is ntg. The u-test was used for CTL vs BTN and ntg CTL vs ntg BTN. The t-test was performed for tg CTL vs tg BTN, BTN vs tg BTN, and tg BTN vs ntg BTN.

(B) Chemotaxis indices of wild type versus *osm-9(ky10),* with or without the transgene *pJK21/$_p$odr-3::GFP::osm-9.* The *$_p$odr-3* promoter drives expression in all three of the pairs of olfactory sensory neurons, including AWA, AWB, and AWC. The *$_p$odr-3* used was the short promoter, 2653 bp in length. The *osm-9* used in the same partial cDNA as in panel A. Data shown from two combined transgenic lines. The Kruskal-Wallis test was used and $p>0.05$.

(C) Chemotaxis indices of wild type versus *osm-9(ky10),* with or without the transgene *KBC24/$_p$odr-3::GFP::osm-9.* The *$_p$odr-3* promoter drives expression in all three of the pairs of olfactory sensory neurons, including AWA, AWB, and AWC. The *$_p$odr-3* used was the long promoter, 2686 bp in length. The *osm-9* used in the same partial cDNA as

in panel A. Data shown from three combined transgenic lines. One-way ANOVA was performed, followed by Bonferroni correction for CTL vs BTN, tg CTL vs tg BTN, ntg CTL vs ntg BTN, BTN vs tg BTN, tg BTN vs ntg BTN, CTL vs tg CTL, and tg CTL vs ntg CTL.

(D) Chemotaxis indices of wild type versus *osm-9(ky10),* with or without the transgene *osm-9::GFP5* [37], which includes the *osm-9* partial cDNA (2497 bp, missing the last 317 bp) driven by the upstream ~1.6 kb promoter and downstream ~3.2 kb promoter, and GFP, cloned into the pBS parent vector. Data shown from three combined transgenic lines. One-way ANOVA was performed, followed by Bonferroni correction for CTL vs BTN, tg CTL vs tg BTN, ntg CTL vs ntg BTN, BTN vs tg BTN, and tg BTN vs ntg BTN.

(E) Chemotaxis indices of wild type versus *osm-9(ky10),* with or without the transgene *KBC42/*$_{p}$*osm-9::osm-9::UTR*, where *posm-9* is the upstream ~1.6 kb promoter, *osm-9* is the full-length cDNA (2814 bp), and *UTR* is the ~3.2 kb downstream promoter. Data shown from three combined transgenic lines. The Kruskal-Wallis test was performed. The u-test was used for CTL vs BTN and ntg CTL vs ntg BTN. The t-test was performed for tg CTL vs tg BTN, BTN vs tg BTN, and BTN tg vs ntg BTN.

(F) Chemotaxis indices of wild type versus *osm-9(ky10),* with or without the transgene WRM065bE12, a ~32 kb fosmid containing the entire *osm-9* gene its upstream and downstream UTR regions. Data shown from two combined transgenic lines. One-way ANOVA was performed, followed by Bonferroni correction for CTL vs BTN, tg CTL vs tg BTN, ntg CTL vs ntg BTN, BTN vs tg BTN, and tg BTN vs ntg BTN.

(G) Chemotaxis indices of wild type versus *osm-9(ky10),* with or without the transgene *KBC38/$_p$nphp-4::osm-9::GFP*. The *$_p$nphp-4* promoter drives expression in all of the ciliated neurons (~60) in the adult worm. The *osm-9* transgene was the full-length cDNA. Data shown from two combined transgenic lines. One-way ANOVA was performed, followed by Bonferroni correction for CTL vs BTN, tg CTL vs tg BTN, ntg CTL vs ntg BTN, BTN vs tg BTN, and tg BTN vs ntg BTN.

S5 Fig. Expressing *osm-9* gDNA under its upstream and downstream endogenous promoters in *ky10* rescues short-term memory. Chemotaxis indices of one-cycle trained animals. *KBC56/$_p$osm-9::osm-9::UTR* is the rescue transgene, where *$_p$osm-9* is the 1.6 kb upstream promoter (Fig 7A), *osm-9* is the full-length gDNA (6342 bp), and UTR is the 3.2 kb downstream promoter (Fig 7A). Teal and blue bars are *osm-9(ky10)* animals expressing *$_p$osm-9::osm-9::UTR* and pink and purple bars are the *osm-9(ky10)* non-transgenic siblings. Uneven number of grey dots because only datasets with N>50 were counted in the graph and analysis. One-way ANOVA was performed, followed by Bonferroni correction for CTL vs BTN, *osm-9(ky10)* + *$_p$osm-9::osm-9::UTR* CTL vs *osm-9(ky10)* + *$_p$osm-9::osm-9::UTR* BTN, *osm-9(ky10)* - *$_p$osm-9::osm-9::UTR* CTL vs *osm-9(ky10)* - *$_p$osm-9::osm-9::UTR* BTN, BTN vs *osm-9(ky10)* + *$_p$osm-9::osm-9::UTR* BTN, *osm-9(ky10)* + *$_p$osm-9::osm-9::UTR* BTN vs *osm-9(ky10)* - *$_p$osm-9::osm-9::UTR* BTN, CTL vs *osm-9(ky10)* + *$_p$osm-9::osm-9::UTR* CTL, and BTN vs *osm-9(ky10)* - *$_p$osm-9::osm-9::UTR* BTN.

To study the expression requirements for *osm-9*/*TRPV5/TRPV6* in classical conditioning, we took a molecular genetic approach by performing rescue experiments

with different *osm-9* transgenes under various promoters in the *osm-9(ky10)* mutant background and compared them to their non-transgenic siblings and wild type as controls. We performed a short-term memory paradigm involving training with and without a food-related odorant for 80 minutes in the absence of food, as previously published [25,51] (S1 Fig). We were unable to rescue the *osm-9(ky10)* odor-learning defect [25] when using a partial *osm-9* cDNA under its endogenous upstream and downstream promoters (S4D Fig), which was previously shown to drive *osm-9* expression and localization [37,38]. We also could not achieve rescue with the cDNA driven by an AWC specific-promoter (*ceh-36*; S4A Fig), the olfactory sensory neuron promoter (*odr-3,* expresses in AWA, AWB, and AWC; S4B and S4C Figs), under both of its own upstream and downstream promoters [37] (S4E Fig), or a ciliated neuron promoter (*nphp-4,* Jauregui and Barr, 2005; S4G Fig). We also could not achieve rescue using a fosmid containing the whole *osm-9* gene (S4F Fig). Partial rescue was achieved using the full-length *osm-9* cDNA under both the olfactory sensory neuron promoter *odr-3* and its own downstream promoter (Fig 6). Full rescue was only obtained when expressing the *osm-9* genomic DNA under both its upstream and downstream promoters, although the extrachromosomal array silenced in all of the transgenic lines after about 4 generations, precluding further rescue analysis (S5 Fig). The significance of the gDNA rescuing the short-term memory defects of *osm-9* mutants may be that the introns contain something required for expression of the *osm-9* gene in order to mediate butanone short-term memory. The fosmid should have also rescued if the introns are indeed required, but it could have been an expression issue that prevented rescue with the fosmid.

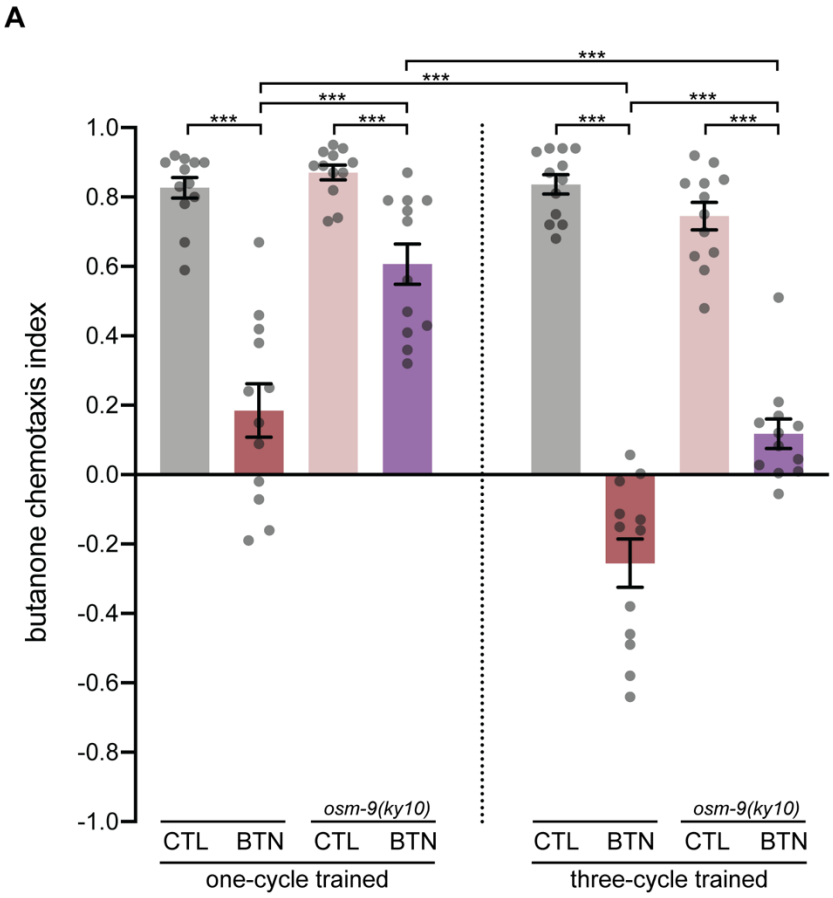

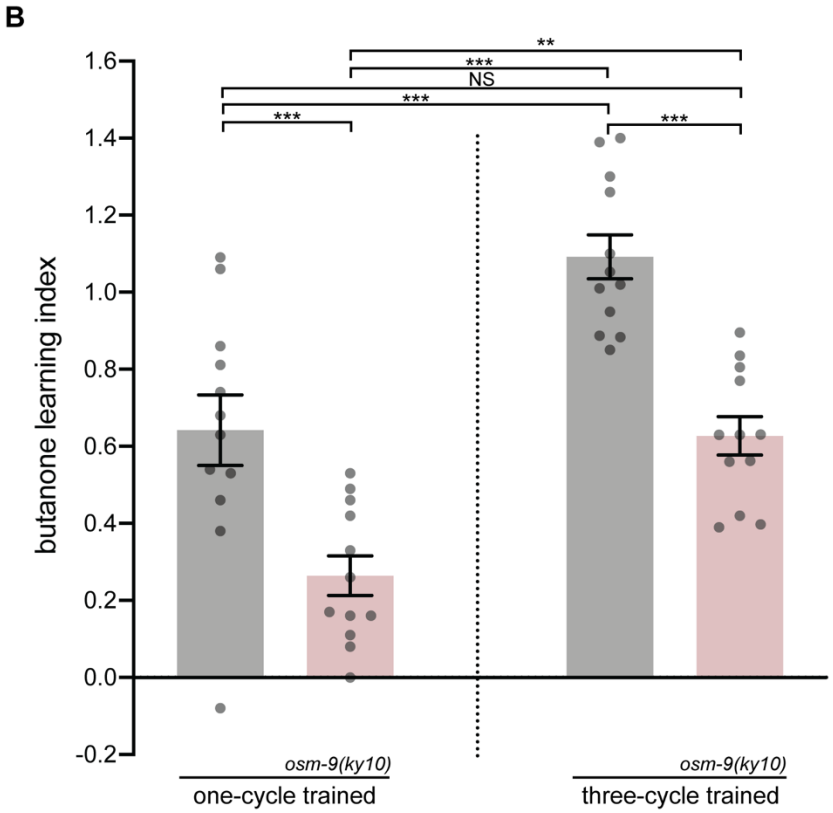

Fig 3.1. The TRPV channel *osm-9* is required for short-term memory, but is not required for memory acquisition post spaced training. (A) Chemotaxis indices for one-cycle odor conditioned and three-cycle odor wild-type vs *osm-9(ky10)* spaced-trained animals. The chemotaxis index (CI) is calculated as the number of worms at the diluent (200-proof ethanol) subtracted from the number at the butanone point source, divided by the total number or worms (excluding any at the origin). Wild-type one- or three-cycle buffer trained (CTL, grey bar), wild-type one- or three-cycle butanone-trained (BTN, red bar), *osm-9(ky10)* one- or three-cycle buffer-trained (CTL, pink bar) and *osm-9(ky10)* one- or three-cycle butanone-trained (BTN, purple bar) are shown, and are denoted this way throughout the rest of the manuscript. “Three-cycle trained” label means 0’ recovery (fifth to eighth bars) and will be annotated this way throughout the paper. N = number of trials where all trials are done on independent days and each grey dot represents an individual assay day, with 50-200 animals/day. The Shapiro-Wilk`` normality test was performed to determine data distribution, and if data were non-normally distributed, the analysis was done with the Kruskal-Wallis test, an analysis of variance of multiple comparisons for non-parametric data. If pairwise comparisons were normally distributed, then p-values were generated with a Student’s unpaired t-test. If any of the datasets were non-parametric, then p-values were generated with the Mann-Whitney u-test. Hochberg adjustment for multiple comparisons was performed on all p-values generated from data included in the same graph to control Type I statistical error. If the data were normally distributed, then one-way ANOVA was performed, followed by Bonferroni correction of pairwise comparisons. Error bars represent S.E.M. Statistical significance was reported as ***p<0.001, ** p< 0.01, *p<0.05, and NS is p>0.05. Behavioral data throughout the paper are represented in this same way with the same numbers of animals on independent days. Additionally, throughout the paper, the same statistical analysis was performed on the data. Note that for every figure in this manuscript, that the Kruskal-Wallis or one-way ANOVA test was performed and yielded ***p<0.001, unless otherwise noted. The Kruskal-Wallis test was performed. The u-test was performed for one-cycle CTL vs BTN, one-cycle *osm-9(ky10)* CTL vs *osm-9(ky10)* BTN, three-cycle trained *osm-9(ky10)* CTL vs *osm-9(ky10)* BTN, one-cycle *osm-9(ky10)* BTN vs three-cycle *osm-9(ky10)* BTN, and three-cycle BTN vs *osm-9(ky10)* BTN. The t-test was performed for one-cycle BTN vs *osm-9(ky10)* BTN, three-cycle CTL vs BTN, and one-cycle BTN vs three-cycle BTN.
(B) Learning indices for one-cycle conditioned and three-cycle spaced-trained wild-type vs *osm-9(ky10)* animals. The learning index (LI) is calculated as the chemotaxis index of the BTN animals subtracted from the chemotaxis index of the CTL animals. The higher the learning index, the more the animals have learned and thus kept the BTN memory. Wild type is shown with grey bars and *osm-9(ky10)* with pink bars, and will be denoted this way throughout the manuscript. One-way ANOVA followed by Bonferroni correction was performed for one-cycle wild type vs *osm-9(ky10)*, one-cycle vs three-cycle wild type, one-cycle wild type vs three-cycle *osm-9(ky10),* one-cycle *osm-9(ky10)* vs three-cycle wild type, one-cycle vs three-cycle *osm-9(ky10)*, and three-cycle wild type vs *osm-9(ky10).*

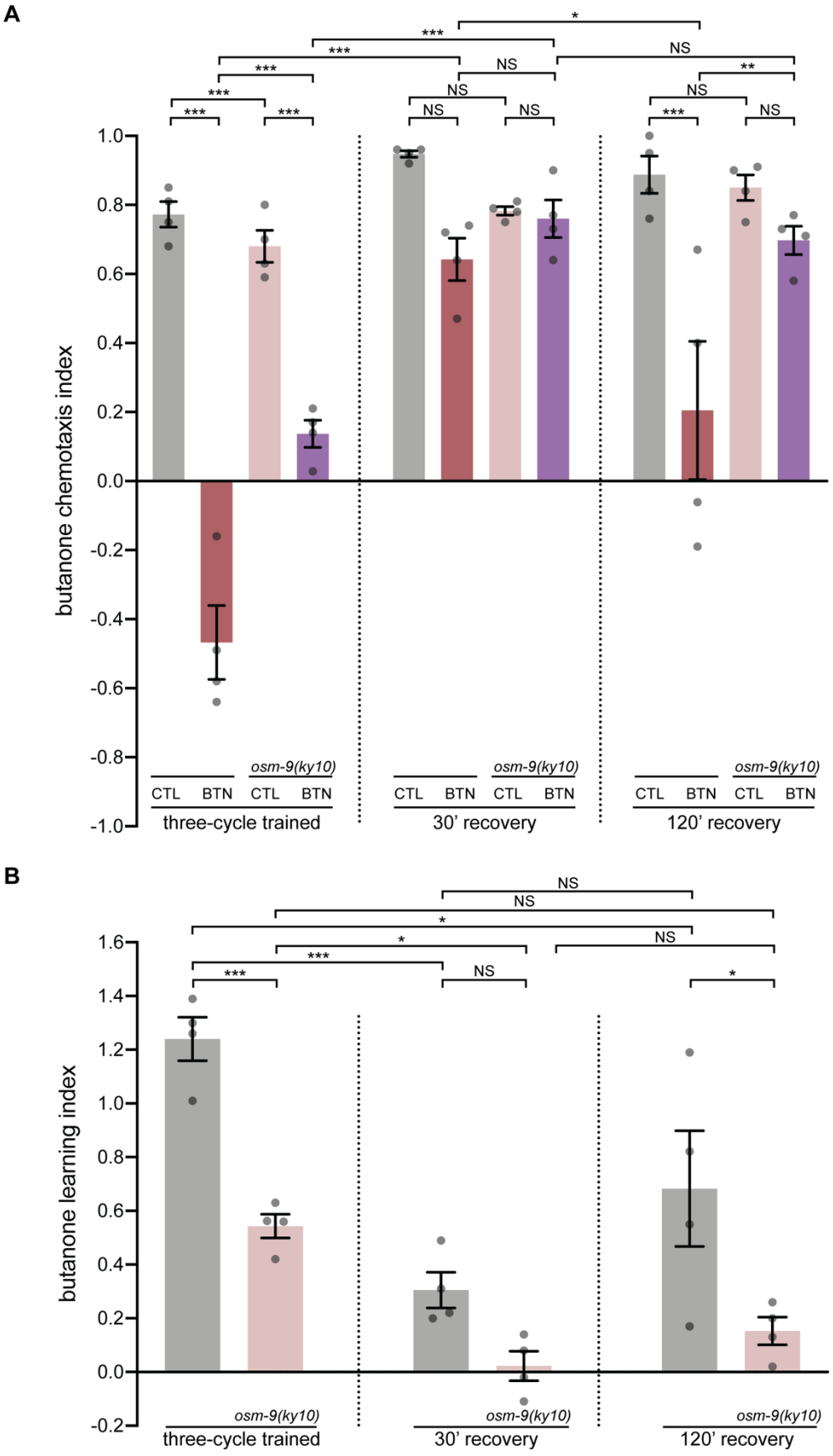

Fig 3.2. The TRPV channel *osm-9* is required for long-term olfactory memory consolidation post spaced training. (A) Chemotaxis indices for three-cycle spaced-trained animals after 0', 30' or 120' post recovery on plates seeded with OP50 as a food source. One-way ANOVA followed by Bonferroni correction was performed for CTL vs BTN, *osm-9(ky10)* CTL vs *osm-9(ky10)* BTN, CTL 30' vs BTN 30', *osm-9(ky10)* CTL 30' vs *osm-9(ky10)* BTN 30', CTL 120' vs BTN 120', *osm-9(ky10)* CTL 120' vs *osm-9(ky10)* BTN 120', CTL vs *osm-9(ky10)* CTL, BTN vs *osm-9(ky10)* BTN, CTL 30' vs *osm-9(ky10)* CTL 30', BTN 30' vs *osm-9(ky10)* BTN 30', CTL 120' vs *osm-9(ky10)* CTL 120', BTN 120' vs *osm-9(ky10)* BTN 120', BTN vs BTN 30', *osm-9(ky10)* BTN vs *osm-9(ky10)* BTN 30', BTN 30' vs BTN 120', and *osm-9(ky10)* BTN 30' vs *osm-9(ky10)* BTN 120'. (B) Learning indices for three-cycle spaced-trained animals after 0', 30', or 120' recovery on food. One-way ANOVA followed by Bonferroni correction was performed for wild-type vs *osm-9(ky10)* after 0' recovery (compare first two bars), 30' recovery (compare third and fourth bars), 120' recovery (compare fifth and sixth bars), wild-type 0' vs 30' *osm-9(ky10)* 0' vs 30', *osm-9(ky10)* 30' vs 120', wild-type 0' vs 120', *osm-9(ky10)* 0' vs 120', and wild-type 30' vs 120', all after three-cycle spaced-training.

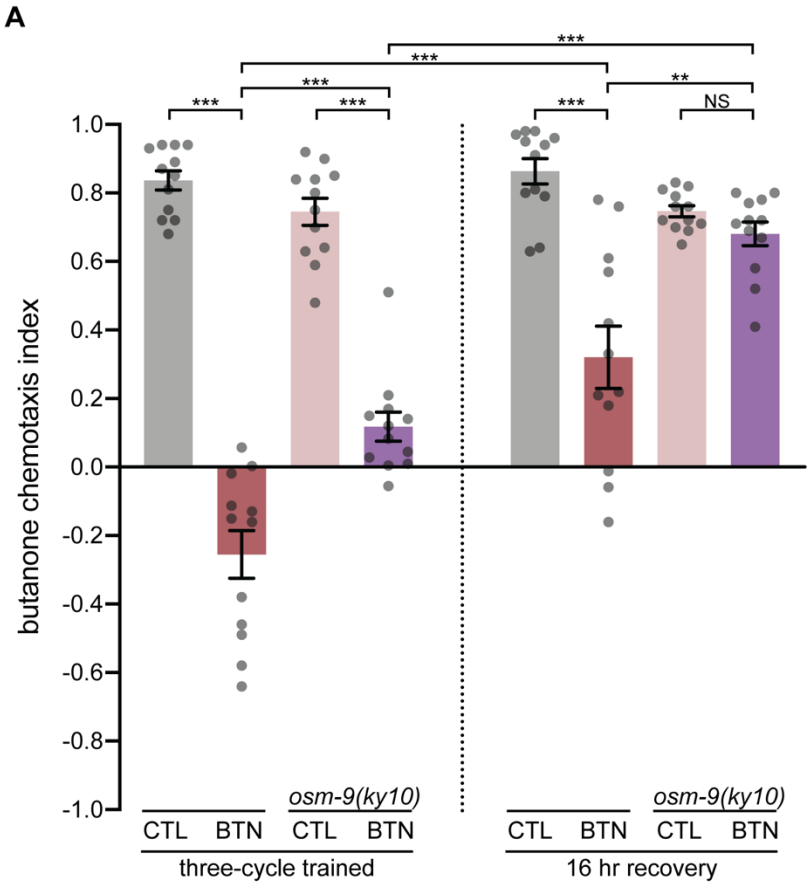

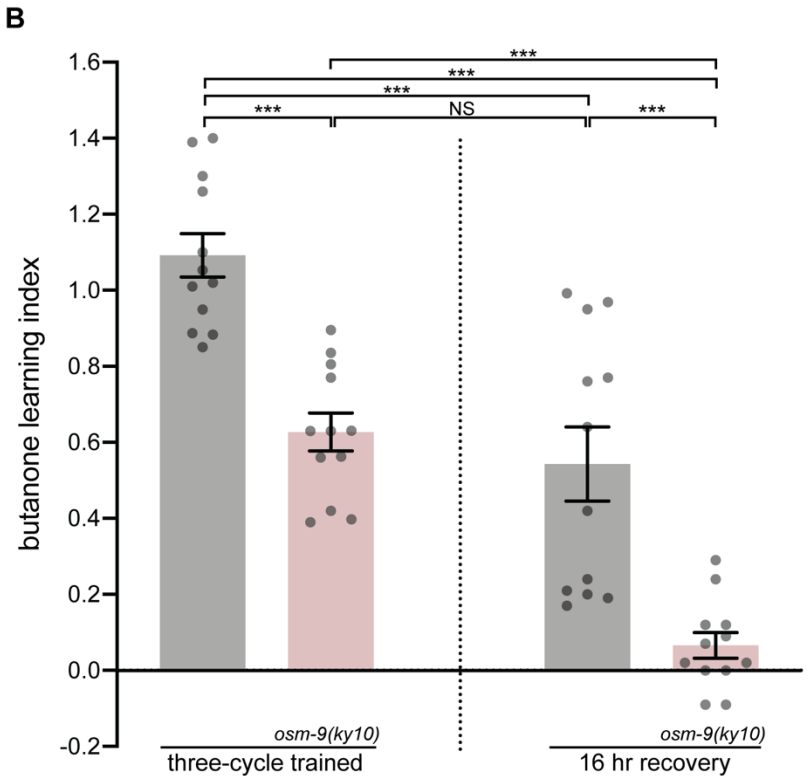

Fig 3.3. *osm-9* animals do not maintain the memory 16 hours after training. (A) Chemotaxis indices for three-cycle trained animals after 0' vs 16 hours of recovery on food. The Kruskal-Wallis test was performed. The u-test was performed for *osm-9(ky10)* CTL vs *osm-9(ky10)* BTN, CTL 16 hr vs BTN 16 hr, *osm-9(ky10)* BTN vs *osm-9(ky10)* BTN 16hr, and BTN vs *osm-9(ky10)* BTN. The t-test was performed for CTL vs BTN, BTN 16 hr vs *osm-9(ky10)* BTN 16 hr, *osm-9(ky10)* CTL 16 hr vs *osm-9(ky10)* BTN 16 hr, and BTN vs BTN 16 hr.
(B) Learning indices for three-cycle trained animals after 0' vs 16 hours of recovery on food. The Kruskal-Wallis test was performed. The u-test was performed for wild type 16 hr vs *osm-9(ky10)* 16 hr, wild type 0' vs wild type 16 hr, and *osm-9(ky10)* 0' vs wild type 16 hr. The t-test was performed for wild type 0' vs *osm-9(ky10)* 0', *osm-9(ky10)* 0' vs *osm-9(ky10)* 16 hr, and wild type 0' vs *osm-9(ky10)* 16 hr.

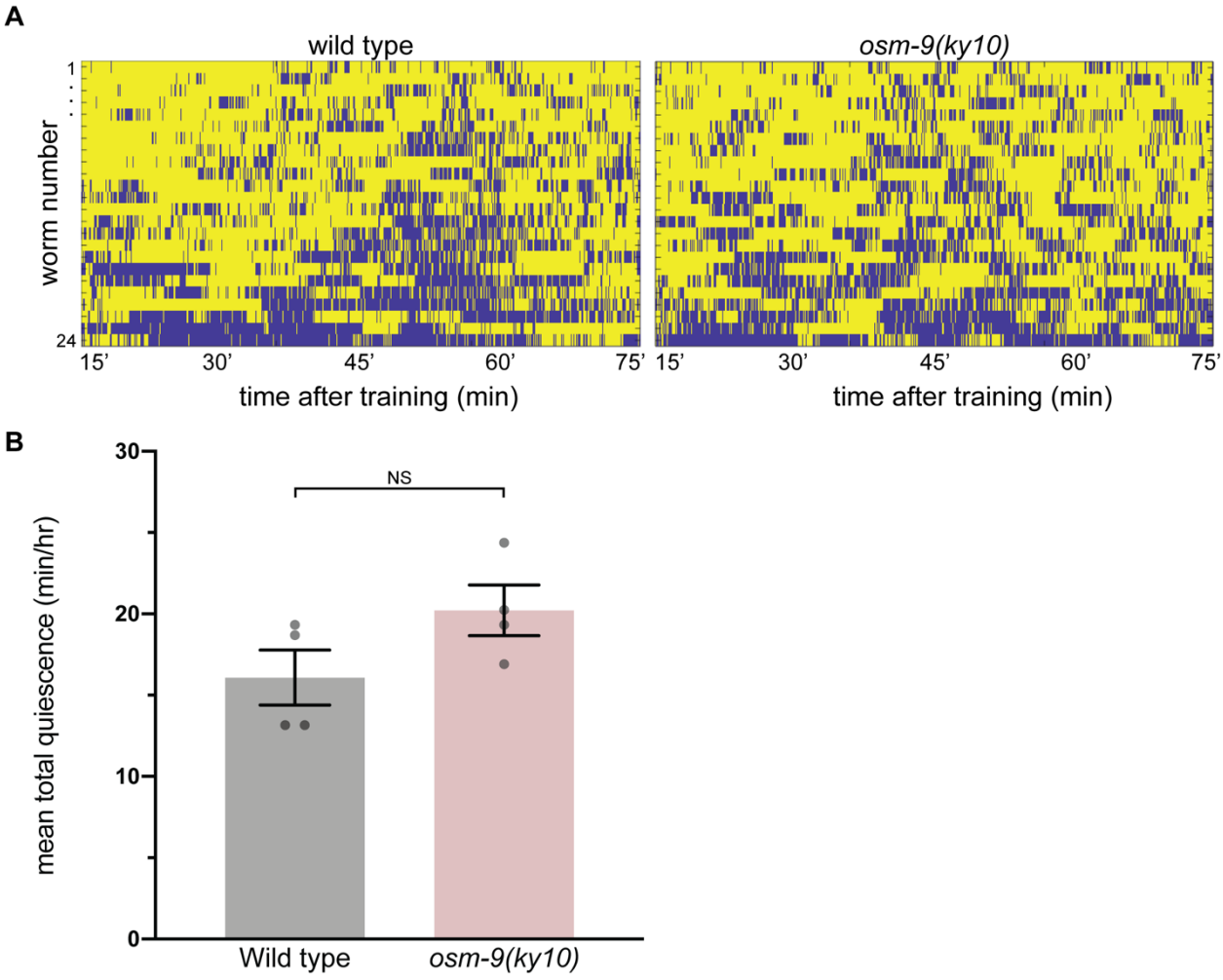

Fig 3.4. Spaced-training does not induce a difference in quiescence between wild type versus *osm-9(ky10)* in the hour post training. (A) Raster plot of activity of wild-type and *osm-9(ky10)* animals 15-75 minutes after three-cycle spaced training. Animals were placed in a WorMotel (Churgin et al., 2017) and videos were taken of their movement. Worm number is shown on the y-axis where each row represents one worm, with 24 worms total shown per plot. Yellow indicates activity and blue indicates quiescence, which was defined as no movement for more than 30 seconds.
(B) The mean total quiescence after spaced training is not significantly different between wild-type and *osm-9(ky10)* animals. Mean total quiescence in minutes per hour of animals in a WorMotel. Each grey dot represents 24 animals tested per condition on an independent day. The t-test was performed.

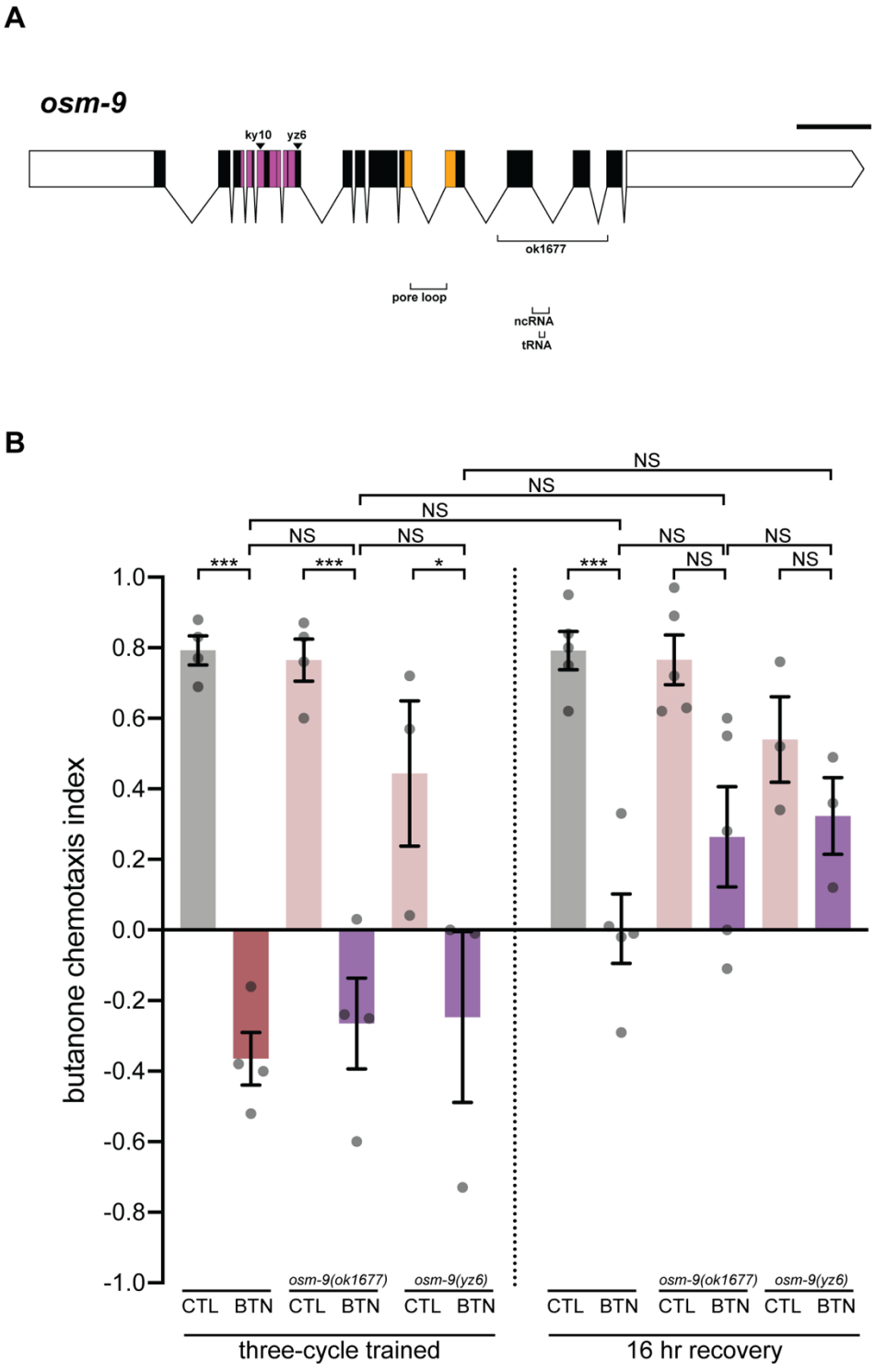

Fig 3.5. The *osm-9(ok1677)* and *osm-9(yz6)* animals can acquire, but cannot maintain long-term memory. (A) Gene map of *osm-9.* Exons are denoted by black boxes and introns are black lines connecting the exons. Red-violet indicates ankyrin repeats (six total). Orange indicates a PKD channel domain. The 5' end white box represents an ~1.6 kb promoter region (Colbert et al., 1997). The 3' end white box

represents an ~3.2 kb promoter region (Colbert et al., 1997). Scale bar indicates 1000 bases. Black arrowheads indicate alleles with point mutations producing early stop codons (*ky10* and *yz6*). The bracket labeled *ok1677* denotes a deletion allele. The brackets labeled ncRNA and tRNA are predicted RNAs produced from these regions. The bracket labeled pore loop denotes the region permeable to calcium, located between the fifth and sixth transmembrane domains.
(B) Chemotaxis indices for three-cycle trained animals with no recovery or 16 hours recovery on food for wild-type, *osm-9(ok1677)* and *osm-9(yz6)* animals. Grey and red bars are wild-type buffer- and butanone-trained animals and pink and purple are *osm-9* buffer- and butanone-trained animals. One-way ANOVA, followed by Bonferroni correction was performed for three-cycle CTL vs BTN, three-cycle *osm-9(ok1677)* CTL vs *osm-9(ok1677)* BTN, three-cycle *osm-9(yz6)* CTL vs *osm-9(yz6)* BTN, 16 hr CTL vs BTN, 16 hr *osm-9(ok1677)* CTL vs *osm-9(ok1677)* BTN, 16 hr *osm-9(yz6)* CTL vs *osm-9(yz6)* BTN, three-cycle BTN vs three-cycle *osm-9(ok1677)* BTN, three-cycle *osm-9(ok1677)* BTN vs three-cycle *osm-9(yz6)* BTN, 16 hr BTN vs 16 hr *osm-9(ok1677)* BTN, 16 hr *osm-9(ok1677)* BTN vs 16 hr *osm-9(yz6)* BTN, three-cycle BTN vs 16 hr BTN, three-cycle *osm-9(ok1677)* BTN vs 16 hr *osm-9(ok1677)* BTN, and three-cycle *osm-9(yz6)* BTN vs 16 hr *osm-9(yz6)* BTN.

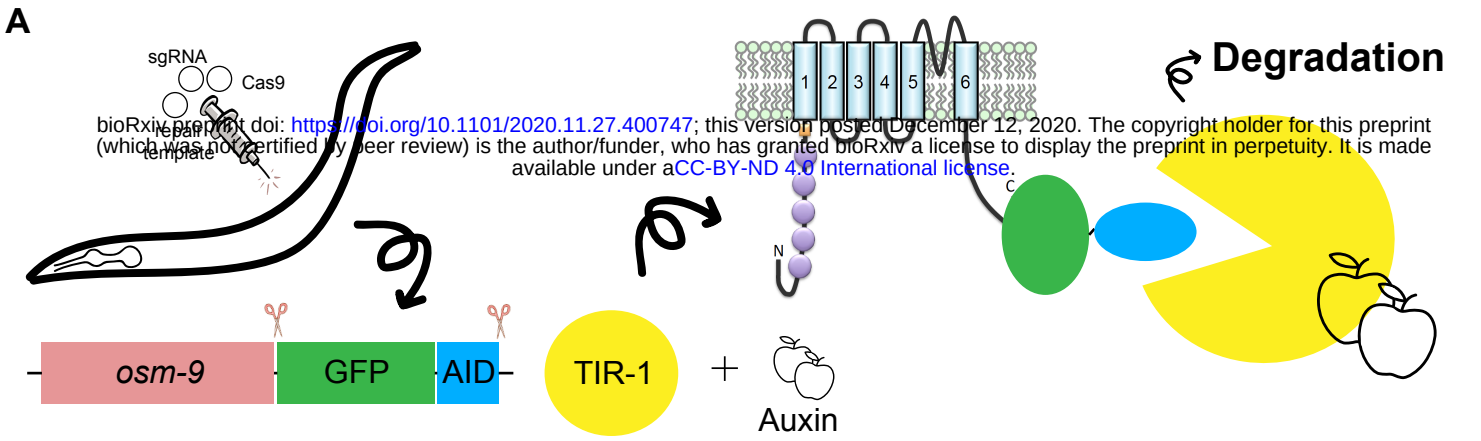

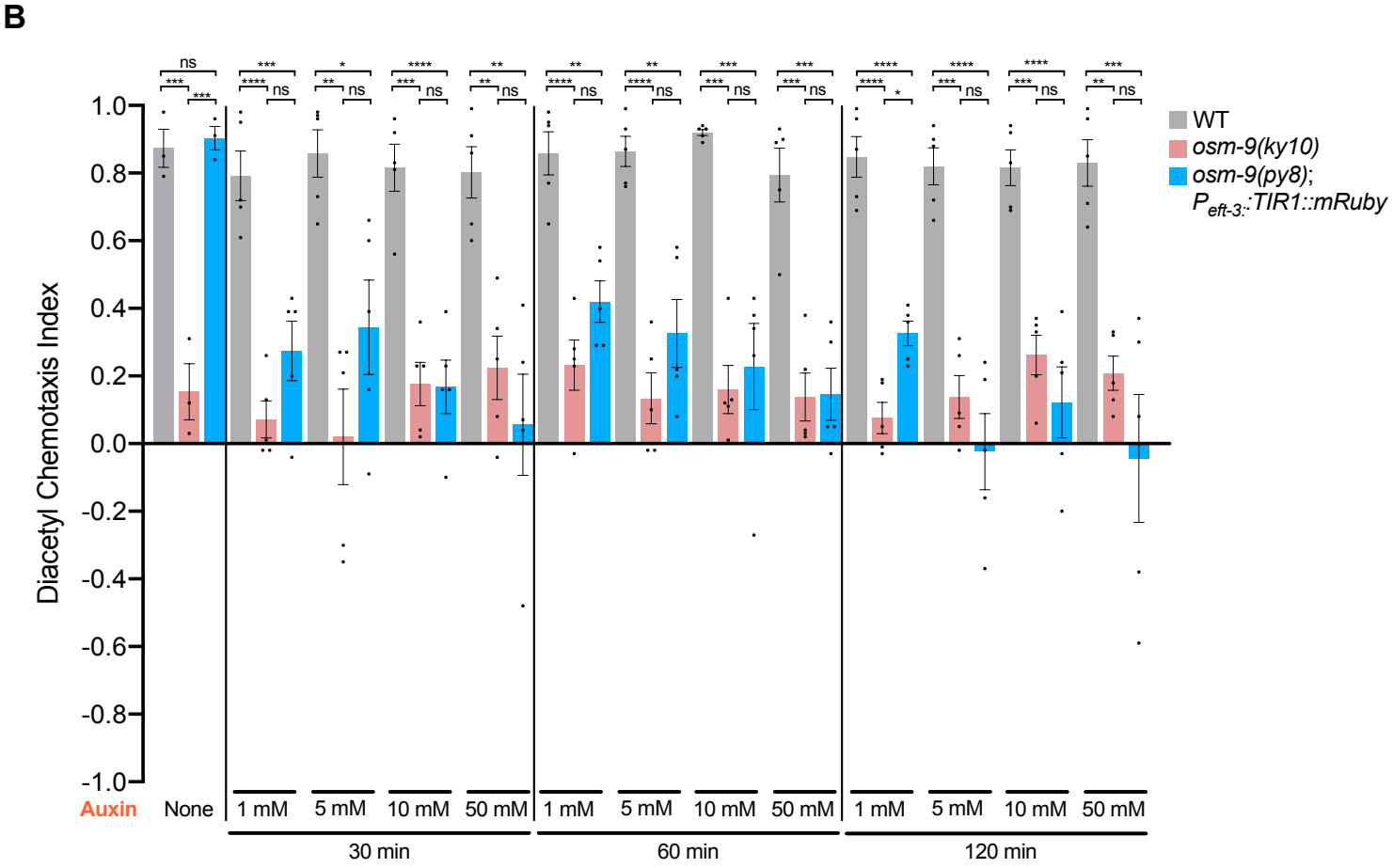

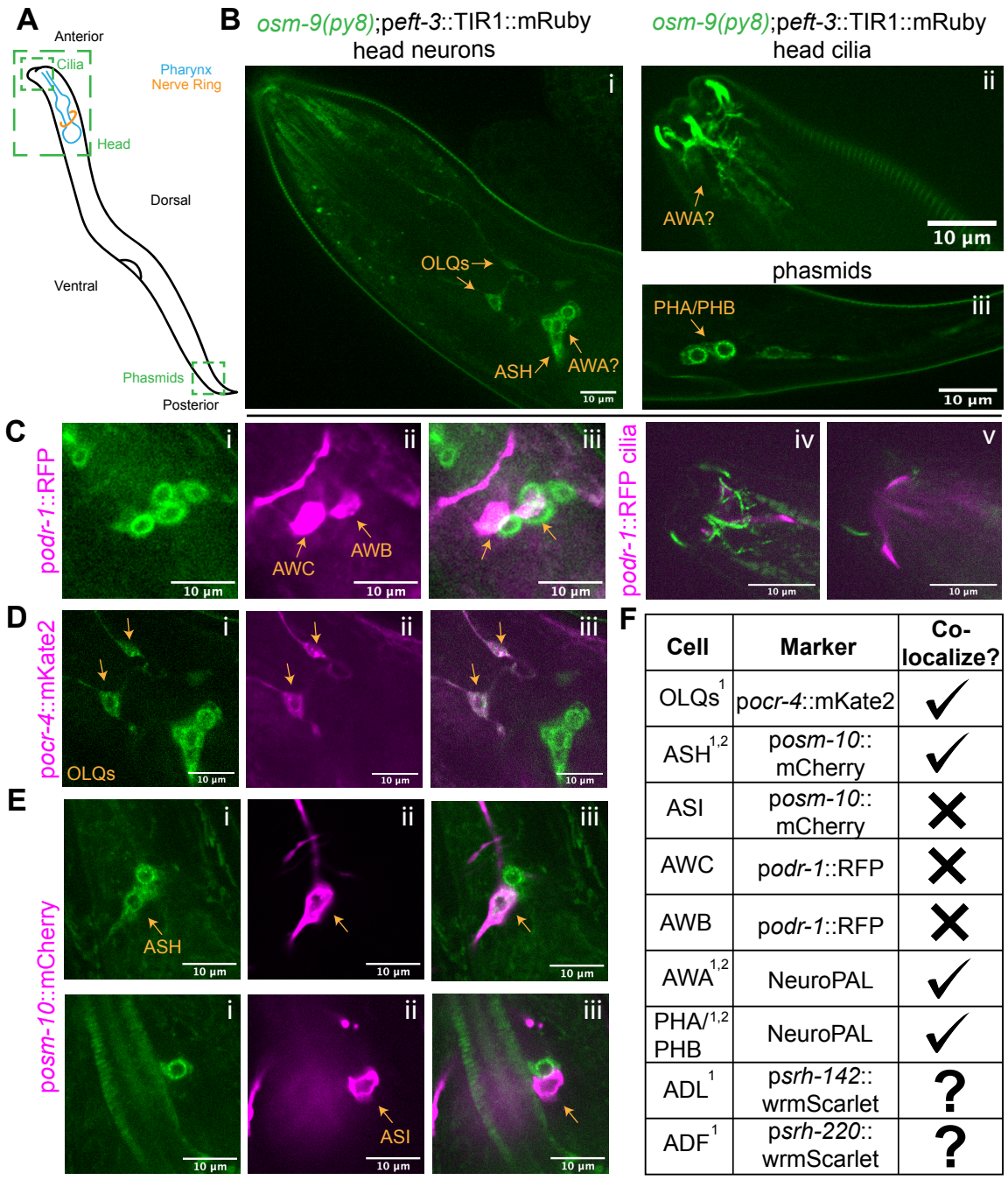

F

Cell	Marker	Co-localize?
OLQs[1]	p*ocr-4*::mKate2	✓
ASH[1,2]	p*osm-10*:: mCherry	✓
ASI	p*osm-10*:: mCherry	✗
AWC	p*odr-1*::RFP	✗
AWB	p*odr-1*::RFP	✗
AWA[1,2]	NeuroPAL	✓
PHA/PHB[1,2]	NeuroPAL	✓
ADL[1]	p*srh-142*:: wrmScarlet	?
ADF[1]	p*srh-220*:: wrmScarlet	?

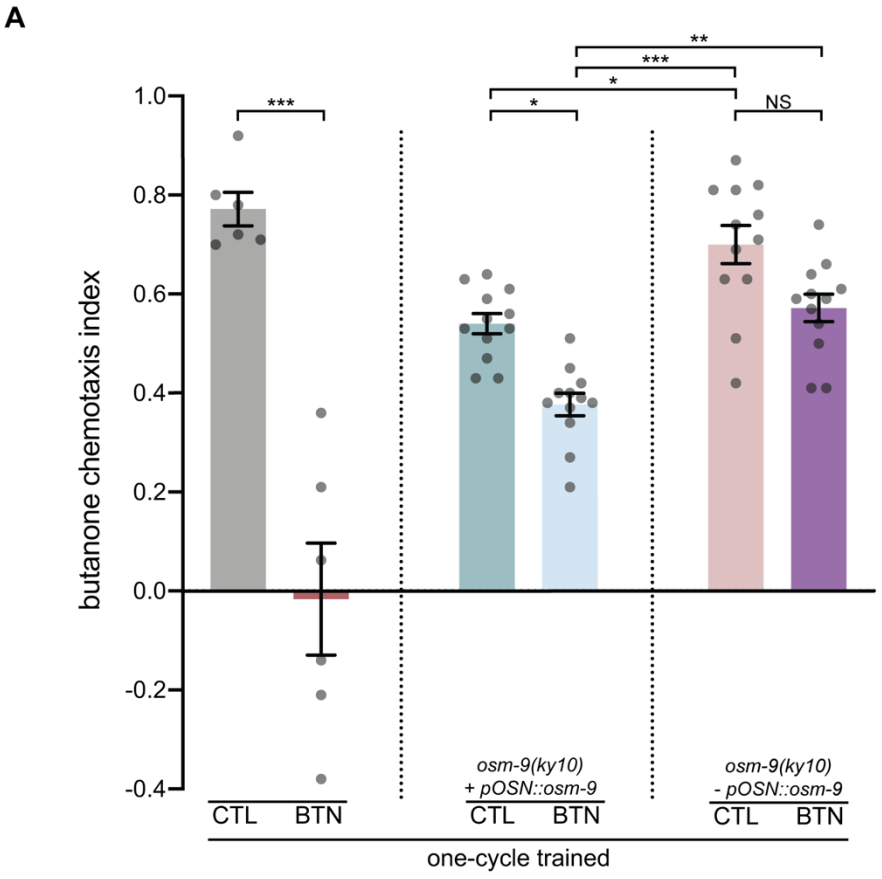

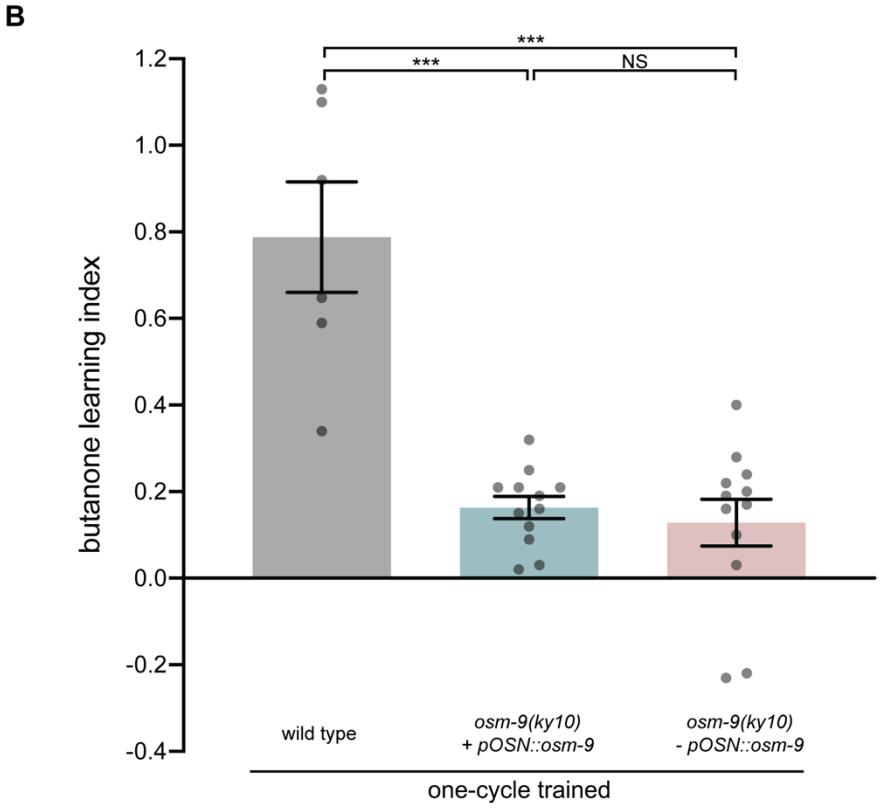

Fig 3.6. Expressing *osm-9* cDNA under the endogenous and OSN promoters in the *ky10* background only partially rescues short-term memory defects. (A) Chemotaxis indices of one-cycle trained animals. Chemotaxis indices of one 80-minute cycle buffer (CTL, first bar, grey) vs butanone-trained (BTN, second bar, red) wild-type animals, buffer-trained (CTL, third bar, teal) vs butanone-trained (BTN, fourth bar, light blue) *osm-9(ky10) IV;* $_p$*OSN::osm-9* animals, and buffer-trained (CTL, fifth bar, pink) vs butanone-trained (BTN, sixth bar, purple) non-transgenic siblings. The transgene is *KBC41/*$_p$*OSN::osm-9::UTR.* The $_p$*OSN* is the $_p$*odr-3* olfactory sensory neuron promoter, driving expression in the AWA, AWB, and AWC neurons, *osm-9* is the full length cDNA (~2.8 kb), and is also driven by the 3' UTR downstream endogenous promoter (~3.2 kb) shown to drive expression in various sensory neurons (Colbert et al., 1997). Transgenic data is from two combined lines. For Fig 1A, one-way ANOVA was performed, followed by the Bonferroni correction for multiple comparisons for CTL vs BTN, CTL vs BTN *osm-9(ky10); +*$_p$*OSN::osm-9*, CTL vs BTN *osm-9(ky10); -* $_p$*OSN::osm-9* (non-transgenic siblings), CTL *osm-9(ky10); +*$_p$*OSN::osm-9* vs CTL *osm-9(ky10); -*$_p$*OSN::osm-9*, BTN *osm-9(ky10); +*$_p$*OSN::osm-9* vs CTL *osm-9(ky10); -*$_p$*OSN::osm-9*, and BTN *osm-9(ky10); +*$_p$*OSN::osm-9* vs BTN *osm-9(ky10); -*$_p$*OSN::osm-9.*
(B) Learning indices for the odor-conditioned animals. One-way ANOVA followed by Bonferroni correction for wild type (first bar, grey) vs *osm-9(ky10); +*$_p$*OSN::osm-9* (second bar, teal), *osm-9(ky10); +*$_p$*OSN::osm-9* vs *osm-9(ky10); -*$_p$*OSN::osm-9* (third bar, pink), and wild type vs *osm-9(ky10); -*$_p$*OSN::osm-9*.

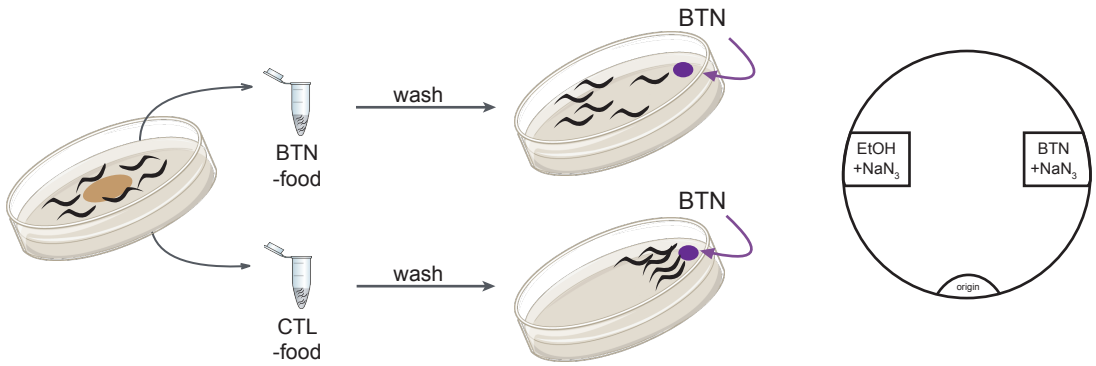

Fig 3.S1. Schematic of one-cycle odor-conditioning. Animals are conditioned to butanone as previously published (Juang et al., 2013). In brief, age-synchronized, one-day old adult animals are washed with buffer from NGM plates containing OP50 food to tubes with either buffer or butanone, both containing no food, for 80 minutes. After the 80-minute incubation, animals are washed and then plated onto chemotaxis assay plates. The chemotaxis index (See Fig 1 legend) is then calculated after at least two hours of the animals roaming.

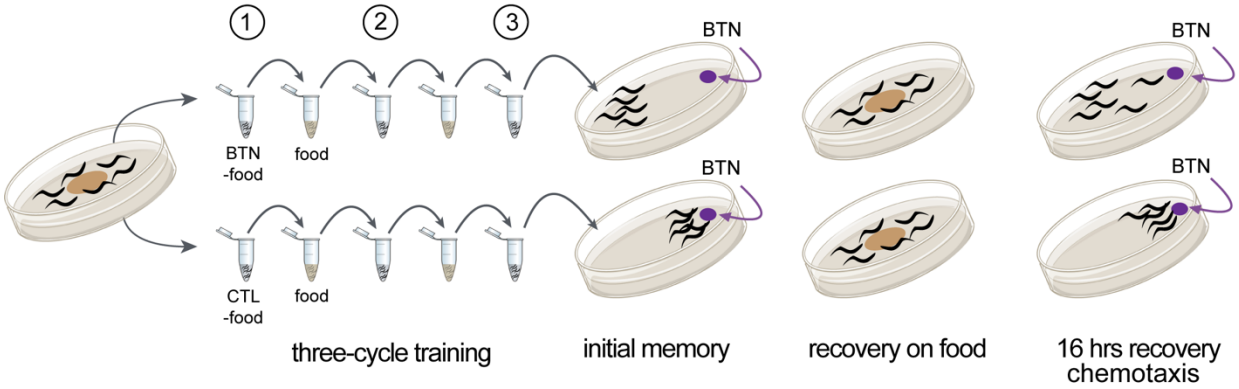

Fig 3.S2 Spaced-training paradigm. Schematic of associative olfactory memory assay to induce long-term odor memory. Age-synchronized, one-day old adult animals are washed from plates with food into tubes and are conditioned to either buffer (CTL) or butanone (BTN) for 80 minutes per cycle in the absence of food for three cycles total, with a 30-minute recovery on food (OP50, OD = 10) in between cycles. After spaced-training, animals are either tested in a butanone chemotaxis assay or are recovered on OP50-seeded NGM plates and then tested.

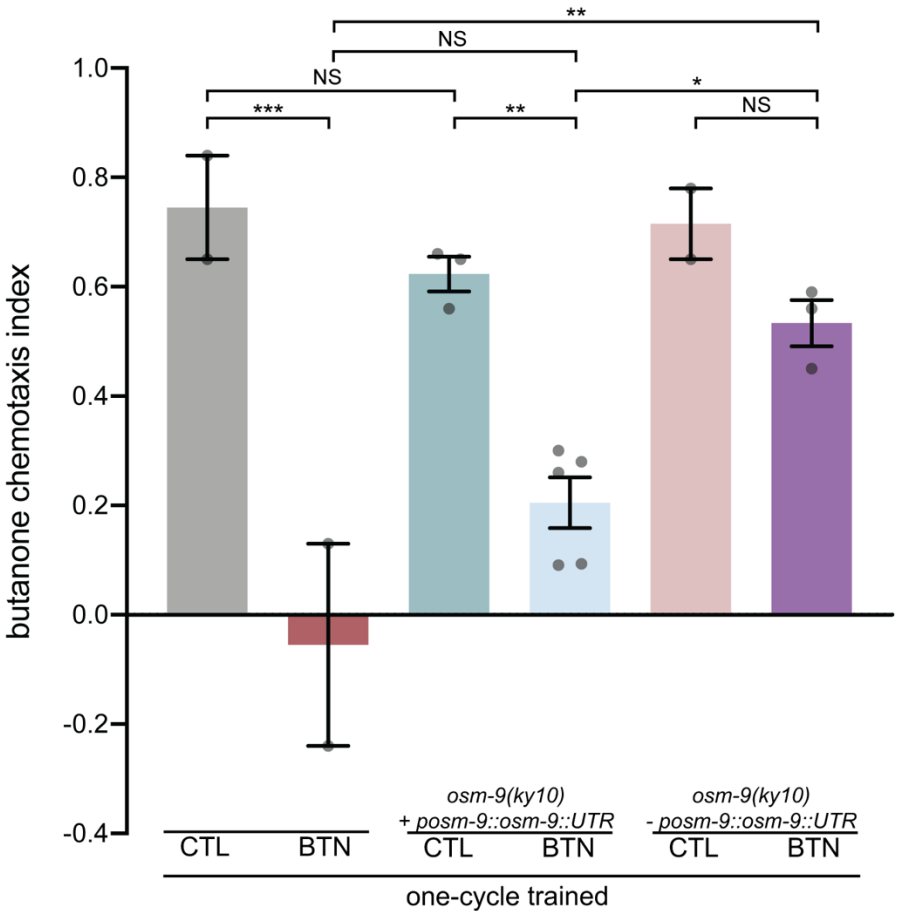

Fig 3.S3. Expressing *osm-9* gDNA under its upstream and downstream endogenous promoters in the *ky10* background rescues short-term memory defects. Chemotaxis indices of one-cycle trained animals. *KBC56/*$_p$*osm-9::osm-9::UTR* is the rescue transgene, where $_p$*osm-9* is the 1.6 kb upstream promoter (Fig 7A), *osm-9* is the full-length gDNA (6342 bp), and UTR is the 3.2 kb downstream promoter (Fig 7A). Teal and blue bars are *osm-9(ky10)* animals expressing $_p$*osm-9::osm-9::UTR* and pink and purple bars are the *osm-9(ky10)* non-transgenic siblings. Uneven number of grey dots because only datasets with N>50 were counted in the graph and analysis. One-way ANOVA was performed, followed by Bonferroni correction for CTL vs BTN, *osm-9(ky10)* + $_p$*osm-9::osm-9::UTR* CTL vs *osm-9(ky10)* + $_p$*osm-9::osm-9::UTR* BTN, *osm-9(ky10)* - $_p$*osm-9::osm-9::UTR* CTL vs *osm-9(ky10)* - $_p$*osm-9::osm-9::UTR* BTN, BTN vs *osm-9(ky10)* + $_p$*osm-9::osm-9::UTR* BTN, *osm-9(ky10)* + $_p$*osm-9::osm-9::UTR* BTN vs *osm-9(ky10)* - $_p$*osm-9::osm-9::UTR* BTN, CTL vs *osm-9(ky10)* + $_p$*osm-9::osm-9::UTR* CTL, and BTN vs *osm-9(ky10)* - $_p$*osm-9::osm-9::UTR* BTN.

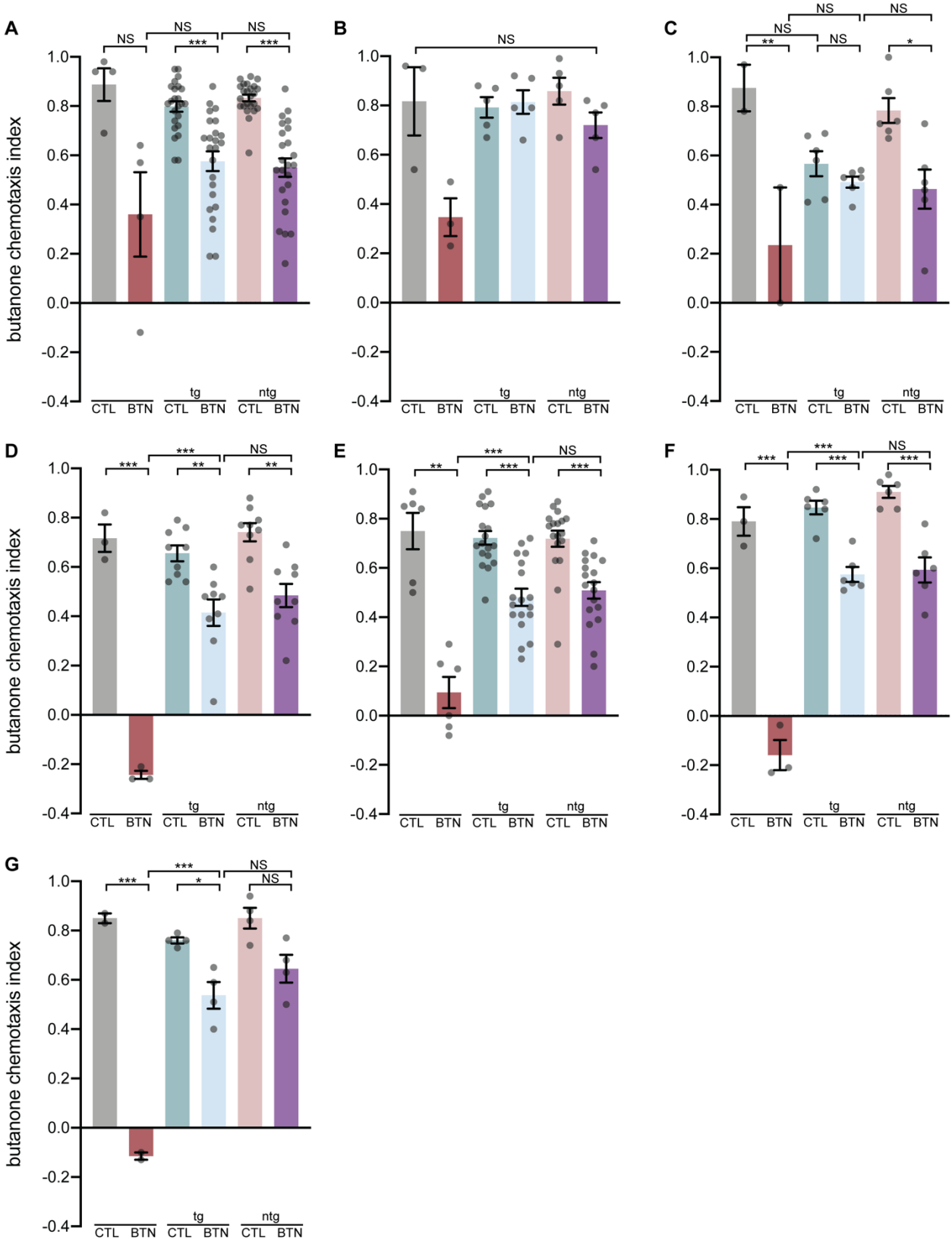

Fig 3.S4. Various *osm-9* expression transgenes are not sufficient to achieve rescue of *osm-9(ky10)* one-cycle butanone conditioning defects. (A) Chemotaxis

indices of wild type versus *osm-9(ky10),* with or without the transgene *KBC8/$_p$ceh-36::osm-9SS::GFP::osm-9.* The *pceh-36* is a promoter driving expression in both of the AWC olfactory sensory neurons. The *osm-9SS* (signal sequence) cDNA was 5' of the GFP and the rest of the cDNA was 3' of the GFP. Data shown from six combined transgenic lines. The Kruskal-Wallis test was performed. Transgenic is tg and non-transgenic is ntg. The u-test was used for CTL vs BTN and ntg CTL vs ntg BTN. The t-test was performed for tg CTL vs tg BTN, BTN vs tg BTN, and tg BTN vs ntg BTN.
(B) Chemotaxis indices of wild type versus *osm-9(ky10),* with or without the transgene *pJK21/$_p$odr-3::GFP::osm-9.* The *$_p$odr-3* promoter drives expression in all three of the pairs of olfactory sensory neurons, including AWA, AWB, and AWC. The *$_p$odr-3* used was the short promoter, 2653 bp in length. The *osm-9* used in the same partial cDNA as in panel A. Data shown from two combined transgenic lines. The Kruskal-Wallis test was used and p>0.05.
(C) Chemotaxis indices of wild type versus *osm-9(ky10),* with or without the transgene *KBC24/$_p$odr-3::GFP::osm-9.* The *$_p$odr-3* promoter drives expression in all three of the pairs of olfactory sensory neurons, including AWA, AWB, and AWC. The *$_p$odr-3* used was the long promoter, 2686 bp in length. The *osm-9* used in the same partial cDNA as in panel A. Data shown from three combined transgenic lines. One-way ANOVA was performed, followed by Bonferroni correction for CTL vs BTN, tg CTL vs tg BTN, ntg CTL vs ntg BTN, BTN vs tg BTN, tg BTN vs ntg BTN, CTL vs tg CTL, and tg CTL vs ntg CTL.
(D) Chemotaxis indices of wild type versus *osm-9(ky10),* with or without the transgene *osm-9::GFP5* (Colbert et al., 1997), which includes the *osm-9* partial cDNA (2497 bp, missing the last 317 bp) driven by the upstream ~1.6 kb promoter and downstream ~3.2 kb promoter, and GFP, cloned into the pBS parent vector. Data shown from three combined transgenic lines. One-way ANOVA was performed, followed by Bonferroni correction for CTL vs BTN, tg CTL vs tg BTN, ntg CTL vs ntg BTN, BTN vs tg BTN, and tg BTN vs ntg BTN.
(E) Chemotaxis indices of wild type versus *osm-9(ky10),* with or without the transgene *KBC42/$_p$osm-9::osm-9::UTR*, where *posm-9* is the upstream ~1.6 kb promoter, *osm-9* is the full-length cDNA (2814 bp), and *UTR* is the ~3.2 kb downstream promoter. Data shown from three combined transgenic lines. The Kruskal-Wallis test was performed. The u-test was used for CTL vs BTN and ntg CTL vs ntg BTN. The t-test was performed for tg CTL vs tg BTN, BTN vs tg BTN, and BTN tg vs ntg BTN.
(F) Chemotaxis indices of wild type versus *osm-9(ky10),* with or without the transgene WRM065bE12, a ~32 kb fosmid containing the entire *osm-9* gene its upstream and downstream UTR regions. Data shown from two combined transgenic lines. One-way ANOVA was performed, followed by Bonferroni correction for CTL vs BTN, tg CTL vs tg BTN, ntg CTL vs ntg BTN, BTN vs tg BTN, and tg BTN vs ntg BTN.
(G) Chemotaxis indices of wild type versus *osm-9(ky10),* with or without the transgene *KBC38/$_p$nphp-4::osm-9::GFP.* The *$_p$nphp-4* promoter drives expression in all of the ciliated neurons (~60) in the adult worm. The *osm-9* transgene was the full-length cDNA. Data shown from two combined transgenic lines. One-way ANOVA was performed, followed by Bonferroni correction for CTL vs BTN, tg CTL vs tg BTN, ntg CTL vs ntg BTN, BTN vs tg BTN, and tg BTN vs ntg BTN.

MATERIALS AND METHODS

Strains and genetics

Strains were maintained by standard methods (Brenner, 1974) and were grown on either 5.5 cm or 10 cm Petri dishes with NGM media seeded with OP50 *E. coli*. All strains were grown at and assayed at 20°C. The wild-type strain is the *C. elegans* N2 Bristol variant. Mutants used in the study include *osm-9(ky10) IV* (Colbert and Bargmann, 1995)*, osm-9(ok1677) IV,* and *osm-9(yz6) IV.* All rescue experiments (**Fig 3.1, Fig 3.S2, Fig 3.S4**) were performed in the *osm-9(ky10) IV* background. The transgenic lines used for the rescue experiments are JZ1967 and JZ1968 [*KBC41/$_p$odr-3::osm-9::UTR* (50 ng/µl), *$_p$unc-122::mCherry* (20 ng/µl)], (**Fig 3.1**); JZ2034, JZ2035, and JZ2036 [*KBC56/$_p$osm-9::osm-9::UTR* (50 ng/µl), *pCFJ90/pmyo-2::mCherry* (2.5 ng/µl), *pSMdelta* (100 ng/µl)], (**Fig 3.S2**); JZ1655 and JZ1656 [*KBC8/$_p$ceh-36::GFP::osm-9* (100 ng/µl), *$_p$unc-122::GFP* (20 ng/µl)], (**Fig 3.S4A**); JZ1621 and JZ1622 [*pJK21/$_p$odr-3::GFP::osm-9* (50 ng/µl), *$_p$unc-122::mCherry* (20ng/µl), ScaI-digested N2 DNA (30 ng/µl)], (**Fig 3.S4B**); JZ1819 and JZ1874 [*KBC24/$_p$odr-3::osm-9* (50 ng/µl), *pCFJ104/$_p$myo-3::mCherry* (5 ng/µl)], (**Fig 3.S4C**); JZ1940 and JZ1941 [fosmid WRM065bE12 (from Source BioScience, 5 ng/µl), *$_p$unc-122::GFP* (20 ng/µl), *$_p$str-2::GCaMP3::mCherry* (25 ng/µl)], (**Fig 3.S4D**); lines containing *osm-9::GFP5* (25 ng/µl), *$_p$unc-122::mCherry* (20 ng/µl), (**Fig 3.S4E**); lines containing *KBC42/$_p$osm-9::osm-9::UTR* (50 ng/µl), *$_p$unc-122::mCherry* (20 ng/µl) or *KBC42/$_p$osm-9::osm-9::UTR* (10 ng/µl), *pCFJ90/$_p$myo-2::mcherry* (2.5 ng/µl), *pSMdelta* (140 ng/µl), (**Fig 3.S4F**); JZ1905 and JZ1906 [*KBC38/$_p$nphp-4::osm-9::GFP* (5 ng/µl), *$_p$unc-122::mCherry* (20 ng/µl); *osm-*

9(ky10) IV gDNA (8 ng/µl); *$_p$ceh-36::mCherry* (5 ng/µl)], (**Fig 3.S4G**). ScaI-digested N2 DNA, *osm-9(ky10) IV* gDNA, or *pSMdelta* (empty vector) were used to bring up the total injection concentration to ensure transgenesis (Evans, 2006). JZ designations are L'Etoile lab strain names.

Molecular Biology

Constructs were made using standard molecular techniques. The construct *pJK21/$_p$odr-3::osm-9SS::GFP::osm-9cDNA* was made by replacing the *$_p$str-2* promoter in *pJK17/$_p$str-2::osm-9SS::GFP::osm-9cDNA*, digested with NotI and AscI restriction enzymes, with the subcloned *$_p$odr-3* fragment from *pJK15/$_p$odr-3::osm-9SS::GFP::osm-9cDNA*, using NotI and AscI. *KBC8/$_p$ceh-36::osm-9SS::GFP::osm-9cDNA* was made by amplifying *$_p$ceh-36* with primers KLB30 (TAACGGCCGGCCTCATCAGCCTACACGTCATC) and KLB31 (ACATAGGCGCGCCCGCAAATGGGCGGAGGGT) to add FseI and AscI sites on and digesting *pAW1/$_p$odr-3::osm-9SS::GFP::osm-9cDNA* with FseI and AscI to remove *$_p$odr-3* and subclone the *$_p$ceh-36* fragment in. *KBC41/$_p$odr-3::osm-9cDNA::UTR* was made by digesting *KBC24/$_p$odr-3::osm-9cDNA* with NheI and NcoI and subcloning in the *osm-9* downstream promoter (~3.2kb), amplified off of phenol-extracted followed by ethanol precipitated whole-worm gDNA (Phenol pH 8 from Sigma Aldrich), using the KLB161 (AGACGCTAGCGAACTTTTTTCTTCTAATTTTTTGA) and KLB162 (AACTCCATGGTTAGGTACATTTAAGGTCGATC) primers, adding on the NheI and NcoI sites. *KBC24/$_p$odr-3::osm-9cDNA* was made by digesting *KBC23/$_p$odr-3* with KpnI and NheI and subcloning in *osm-9* cDNA, amplified from whole-worm cDNA (a kind gift

from Maria Gallegos) using primers KLB25 (AACTGGTACCTCATTCGCTTTTGTCATTTGTC) and KLB90 (AGACGCTAGCATGGGCGGTGGAAGTTCG), which add on the KpnI and NheI sites. *KBC42/$_p$osm-9::osm-9cDNA::UTR* was made by digesting *KBC41/$_p$odr-3::osm-9cDNA::UTR* with NotI and XmaI and subcloning in the upstream *osm-9* promoter (~1.6 kb), amplified off of phenol-extracted followed by ethanol precipitated whole-worm gDNA (Phenol pH 8 from Sigma Aldrich), using the primers KLB163 (AGACGCGGCCGCCGCGGGAGTACTTTACGGG) and KLB164 (AACTCCCGGGGTTTGGTTTCTGAAAAAATTGG), adding on NotI and XmaI sites. *KBC38/$_p$nphp-4::GFP::osm-9* was made by digesting *KBC26/$_p$odr-3::osm-9cDNA::GFP* with NotI and NruI and subcloning in the *nphp-4* promoter amplified from *pAK59/$_p$nphp-4::GFP::npp-19* (a kind gift from Piali Sengupta) with primer KLB127 (AGACGCGGCCGCCAACATTATTAATCACTGCAAC) and KLB128 (AACTTCGCGAACTTCCACCGCCCATCTCATTTTTCGAGACTTTGTTA), adding on NotI and NruI sites. KBC56 was made by the following instructions: osm-9 gDNA was amplified with the primers KLB289 (GTTGTTTACCTTTTATGTTCATCCG) and KLB290 (AAATTTTCTACTGCCTGGTATCAAA) off of phenol-extracted followed by ethanol precipitated whole-worm gDNA (Phenol pH 8 from Sigma Aldrich). The *osm-9* gDNA fragment plus extra upstream and downstream homologous sequence was amplified off of the gDNA amplified with KLB289 and KLB290, using the primers KLB298 (GTTGTTTACCTTTTATGTTCAT) and KLB299 (AAAATGATCCACATAAAATTTTCTACTGCCTGGTAT). The *osm-9* upstream partial fragment (~1.2 kb) was amplified using the primers KLB296

(TGATTACGCCAAGCTTCGCGGGAGTACTTTACGG) and KLB297 (TAAAAGGTAAACAACTAGTTTTTAGTACATGAAATAATT) off of the template KBC42/ *$_p$osm-9::osm-9cDNA::UTR*, and the downstream promoter partial fragment was amplified with KLB300 (TATGTGGATCATTTTTGTCTC) and KLB301 (CCGCGCATGCAAGCTTTTAGGTACATTTAAGGTCGAT) off of KBC42/ *$_p$osm-9::osm-9cDNA::UTR*. The three fragments were then recombined in the *pSM* plasmid (linearized with HindIII) using the Takara Infusion HD Cloning kit. The *pSM* plasmid was from Steve McCarroll.

Chemotaxis assay

We utilized the chemotaxis assay from Bargmann et al., 1993. About 4-5 Larval stage 4 (L4) animals were put onto NGM plates seeded with OP50 *E. coli* for 5 days at 20°C, or until populations are one-day old adults. Any plates with fungal or bacterial contamination were not included in the assays. Animals were then washed off the plates using S. basal buffer and into microfuge tubes (sterile, but not autoclaved), where they were conditioned to either S. basal buffer (0.1M NaCl, 0.05M K_3PO_4, pH 6.0), or 2-butanone (Sigma) diluted in S. basal buffer, 1:10,000 (1.23 mM) concentration. Animals were incubated for 80 minutes on a rotating microfuge tube stand. Next, animals were washed two times with S. basal, where the worms were allowed to pellet (about two to three minutes) without spinning them down. Next, the worms were washed with ddH_2O to ensure all salts were removed, and then placed onto a 10 cm Petri dish chemotaxis plate. The chemotaxis plate media was made by adding 100 mL ddH_2O to 1.6 g of Difco bacto agar, then boiled, and then 500 µl of 1M K_3PO_4, 100 µl 1M $CaCl_2$ and 100 µl 1M

$MgSO_4$ were added, and then the media was pipetted at 10 ml per 10 cm plastic petri dish and let cool to solidify, and then square odor arenas and an origin were drawn (S1 Fig). The chemotaxis plate was made with two point sources – one arena with 1 ul of 200-proof ethanol, and the other arena with 1 µl of 1:1000 butanone in ethanol. Each point source also contained 1 µl of 1M sodium azide (Fisher Scientific) to paralyze worms once they reached the arenas (S1 Fig). Animals were placed at the origin, the liquid was removed with a Kim Wipe, and then animals were allowed to roam for at least two hours. Then, the chemotaxis index or learning index was calculated (Fig 1 legend). For reference, most untrained or buffer-trained wild-type animals have a butanone chemotaxis index from 0.6 to 0.9. If pairwise comparisons between the chemotaxis indices of the buffer-trained and butanone-trained populations of the same genotype were not significantly different from each other, then we deemed them memory defective.

LTM chemotaxis assay

The assay is performed as written above in the “Chemotaxis assay” section, but for three cycles instead of just one, with recovery periods on food in between. Animals are incubated for 80 minutes in either buffer or butanone diluted in buffer. Animals are washed, and then incubated for 30 minutes in OP50 diluted in S. basal buffer (OD = 10). Animals are washed as before, but then conditioned for another 80 minutes in either buffer or diluted butanone, making this the second odor-treatment cycle. Animals are then washed and incubated with OP50 for another 30 minutes, washed, and then subjected to a third buffer or odor conditioning cycle. Animals are then washed as

before, and plated onto chemotaxis plates (this is the 0' recovery, three-cycle trained worms), or recovered on 5.5 cm NGM plates seeded with OP50 for either 30', 120', or 16 hours, where they are then subjected to the chemotaxis assay.

WorMotel assay

The WorMotel (Churgin et al., 2017) was used according to previously published methods, as well as this link with more detailed methods (http://fangyenlab.seas.upenn.edu/links.html). In brief, a 48-well PDMS chip called the WorMotel was filled with media and seeded with OP50 (OD = 10), and one worm was placed into each individual well. Behavior was recorded by video using the Multiple Worm Tracker software (https://sourceforge.net/projects/mwt/) and movement was analyzed with Matlab software (KS_analysis_CFY_Jan2019.m and MC_QuiescenceActivity_v1202.fig, both at https://github.com/cfangyen/LEtoile_WorMotel). Excel sheets with total quiescence for each worm is generated from the Matlab code. The mean total quiescence was then taken for statistical analysis.

Statistical Analysis

All data included in the same graph were subjected to the Shapiro-Wilk normality test. If all of the datasets were normally distributed, then one-way ANOVA was performed, followed by Bonferroni correction for pairwise comparisons. If any datasets were non-normally distributed, then the Kruskal-Wallis test was performed. If $p>0.05$, then no further analysis was performed. If $p<0.05$, then the test was followed up by either the

Mann-Whitney u-test for non-parametric data pairwise comparisons or the Student's unpaired t-test for parametric data pairwise comparisons. All p-values included in the same graph were then adjusted using the Hochberg test to remove any type I statistical error, which prevents incorrect rejection of the null hypothesis. ***p<0.001, **p<0.01, *p<0.05, NS indicates p>0.05. All graphs show S.E.M. Graphpad Prism and R studio were used for all of the statistical tests. Each data point (represented by grey dots) on the graphs indicates one population of 400>N>50, run on independent days.

REFERENCES

Almeida, V., Peres, F.F., Levin, R., Suiama, M.A., Calzavara, M.B., Zuardi, A.W., Hallak, J.E., Crippa, J.A., and Abílio, V.C. (2014). Effects of cannabinoid and vanilloid drugs on positive and negative-like symptoms on an animal model of schizophrenia: The SHR strain. Schizophrenia Research *153*, 150–159.

Bailey, C.H., Kandel, E.R., and Harris, K.M. (2015). Structural Components of Synaptic Plasticity and Memory Consolidation. Cold Spring Harb Perspect Biol *7*, a021758.

Balleza-Tapia, H., Crux, S., Andrade-Talavera, Y., Dolz-Gaiton, P., Papadia, D., Chen, G., Johansson, J., and Fisahn, A. TrpV1 receptor activation rescues neuronal function and network gamma oscillations from Ab-induced impairment in mouse hippocampus in vitro. 24.

Bargmann, C.I., and Horvitz, H.R. (1991). Chemosensory neurons with overlapping functions direct chemotaxis to multiple chemicals in C. elegans. Neuron *7*, 729–742.

Bargmann, C.I., Hartweig, E., and Horvitz, H.R. (1993). Odorant-selective genes and neurons mediate olfaction in C. elegans. Cell *74*, 515–527.

Bashiri, H., Hosseini-Chegeni, H., Alsadat Sharifi, K., Sahebgharani, M., and Salari, A.-A. (2018). Activation of TRPV1 receptors affects memory function and

hippocampal TRPV1 and CREB mRNA expression in a rat model of biliary cirrhosis. Neurological Research *40*, 938–947.

Birnby, D.A., Link, E.M., Vowels, J.J., Tian, H., Colacurcio, P.L., and Thomas, J.H. (2000). A Transmembrane Guanylyl Cyclase (DAF-11) and Hsp90 (DAF-21) Regulate a Common Set of Chemosensory Behaviors in Caenorhabditis elegans. Genetics *155*, 85–104.

Bovet-Carmona, M., Menigoz, A., Pinto, S., Tambuyzer, T., Krautwald, K., Voets, T., Aerts, J.-M., Angenstein, F., Vennekens, R., and Balschun, D. (2018). Disentangling the role of TRPM4 in hippocampus-dependent plasticity and learning: an electrophysiological, behavioral and FMRI approach. Brain Struct Funct *223*, 3557–3576.

Brenner, S. (1974). The genetics of Caenorhabditis elegans. Genetics *77*, 71–94.

Chen, J., Zhang, X.-F., Kort, M.E., Huth, J.R., Sun, C., Miesbauer, L.J., Cassar, S.C., Neelands, T., Scott, V.E., Moreland, R.B., et al. (2008). Molecular Determinants of Species-Specific Activation or Blockade of TRPA1 Channels. Journal of Neuroscience *28*, 5063–5071.

Cho, C.E., Brueggemann, C., L'Etoile, N.D., and Bargmann, C.I. (2016). Parallel encoding of sensory history and behavioral preference during Caenorhabditis elegans olfactory learning. ELife *5*, e14000.

Churgin, M.A., Jung, S.-K., Yu, C.-C., Chen, X., Raizen, D.M., and Fang-Yen, C. (2017). Longitudinal imaging of Caenorhabditis elegans in a microfabricated device reveals variation in behavioral decline during aging. ELife *6*, e26652.

Colbert, H., and Bargmann, C.I. (1995). Odorant-specific adaptation pathways generate olfactory plasticity in C. elegans. Neuron *14*, 803–812.

Colbert, H.A., Smith, T.L., and Bargmann, C.I. (1997). OSM-9, A Novel Protein with Structural Similarity to Channels, Is Required for Olfaction, Mechanosensation, and Olfactory Adaptation in *Caenorhabditis elegans*. J. Neurosci. *17*, 8259–8269.

Cook, S.J., Jarrell, T.A., Brittin, C.A., Wang, Y., Bloniarz, A.E., Yakovlev, M.A., Nguyen, K.C.Q., Tang, L.T.-H., Bayer, E.A., Duerr, J.S., et al. (2019). Whole-animal connectomes of both Caenorhabditis elegans sexes. Nature *571*, 63–71.

Coswna, D.J., and Manning, A. (1969). Abnormal Electroretinogram from a Drosophila Mutant. Nature *224*, 285–287.

Dang, S., van Goor, M.K., Asarnow, D., Wang, Y., Julius, D., Cheng, Y., and van der Wijst, J. (2019). Structural insight into TRPV5 channel function and modulation. Proc Natl Acad Sci USA *116*, 8869–8878.

De Petrocellis, L., Ligresti, A., Moriello, A.S., Allarà, M., Bisogno, T., Petrosino, S., Stott, C.G., and Di Marzo, V. (2011). Effects of cannabinoids and cannabinoid-enriched Cannabis extracts on TRP channels and endocannabinoid metabolic enzymes:

Novel pharmacology of minor plant cannabinoids. British Journal of Pharmacology *163*, 1479–1494.

De Petrocellis, L., Nabissi, M., Santoni, G., and Ligresti, A. (2017). Actions and Regulation of Ionotropic Cannabinoid Receptors. In Advances in Pharmacology, (Elsevier), pp. 249–289.

Di Marzo, V., Gobbi, G., and Szallasi, A. (2008). Brain TRPV1: a depressing TR(i)P down memory lane? Trends in Pharmacological Sciences *29*, 594–600.

Dudai, Y. (1996). Consolidation: Fragility on the Road to the Engram. Neuron *17*, 367–370.

Dudai, Y. (2004). The Neurobiology of Consolidations, Or, How Stable is the Engram? Annu. Rev. Psychol. *55*, 51–86.

Eguchi, N., Hishimoto, A., Sora, I., and Mori, M. (2016). Slow synaptic transmission mediated by TRPV1 channels in CA3 interneurons of the hippocampus. Neuroscience Letters *616*, 170–176.

Evans, T. (2006). Transformation and microinjection. WormBook.

Fox, K., and Stryker, M. (2017). Integrating Hebbian and homeostatic plasticity: introduction. Philosophical Transactions of the Royal Society B *372*.

Genro, B.P., de Oliveira Alvares, L., and Quillfeldt, J.A. (2012). Role of TRPV1 in consolidation of fear memories depends on the averseness of the conditioning procedure. Neurobiology of Learning and Memory *97*, 355–360.

Gibson, H.E., Edwards, J.G., Page, R.S., Van Hook, M.J., and Kauer, J.A. (2008). TRPV1 Channels Mediate Long-Term Depression at Synapses on Hippocampal Interneurons. Neuron *57*, 746–759.

van Goor, M.K.C., Hoenderop, J.G.J., and van der Wijst, J. (2017). TRP channels in calcium homeostasis: from hormonal control to structure-function relationship of TRPV5 and TRPV6. Biochimica et Biophysica Acta (BBA) - Molecular Cell Research *1864*, 883–893.

Gordus, A., Pokala, N., Levy, S., Flavell, S.W., and Bargmann, C.I. (2015). Feedback from network states generates variability in a probabilistic olfactory circuit. Cell *161*, 215–227.

Grueter, B.A., Brasnjo, G., and Malenka, R.C. (2010). Postsynaptic TRPV1 triggers cell type–specific long-term depression in the nucleus accumbens. Nat Neurosci *13*, 1519–1525.

Hall, S.E., Beverly, M., Russ, C., Nusbaum, C., and Sengupta, P. (2010). A Cellular Memory of Developmental History Generates Phenotypic Diversity in C. elegans. Current Biology *20*, 149–155.

Hellmich, U.A., and Gaudet, R. (2014). Structural Biology of TRP Channels. In Mammalian Transient Receptor Potential (TRP) Cation Channels, B. Nilius, and V. Flockerzi, eds. (Cham: Springer International Publishing), pp. 963–990.

Jauregui, A.R., and Barr, M.M. (2005). Functional characterization of the C. elegans nephrocystins NPHP-1 and NPHP-4 and their role in cilia and male sensory behaviors. Experimental Cell Research *305*, 333–342.

Juang, B.-T., Gu, C., Starnes, L., Palladino, F., Goga, A., Kennedy, S., and L'Etoile, N.D. (2013). Endogenous Nuclear RNAi Mediates Behavioral Adaptation to Odor. Cell *154*, 1010–1022.

Julius, D. (2013). TRP channels and pain. Annual Review of Cell and Developmental Biology *29*, 355—384.

Kahn-Kirby, A.H., Dantzker, J.L.M., Apicella, A.J., Schafer, W.R., Browse, J., Bargmann, C.I., and Watts, J.L. (2004). Specific Polyunsaturated Fatty Acids Drive TRPV-Dependent Sensory Signaling In Vivo. Cell *119*, 889–900.

Kaiser, M. (2015). Neuroanatomy: Connectome Connects Fly and Mammalian Brain Networks. Current Biology *25*, R416–R418.

Kang, K., Pulver, S.R., Panzano, V.C., Chang, E.C., Griffith, L.C., Theobald, D.L., and Garrity, P.A. (2010). Analysis of Drosophila TRPA1 reveals an ancient origin for human chemical nociception. Nature *464*, 597–600.

Kaufmann, A.L., Ashraf, J.M., Corces-Zimmerman, R., Landis, J.N., and Murphy, C.T. (2010). Insulin Signaling and Dietary Restriction Differentially Influence the Decline of Learning and Memory with Age. PLOS Biology *8*, e1000372.

Lee, J.I., O'Halloran, D.M., Eastham-Anderson, J., Juang, B.-T., Kaye, J.A., Scott Hamilton, O., Lesch, B., Goga, A., and L'Etoile, N.D. (2010). Nuclear entry of a cGMP-dependent kinase converts transient into long-lasting olfactory adaptation. Proceedings of the National Academy of Sciences *107*, 6016–6021.

Lent, C.M. (1977). Cellular Basis of Behavior. An Introduction to Behavioral Neurobiology. Eric R. Kandel. The Quarterly Review of Biology *52*, 326–327.

L'Etoile, N.D., and Bargmann, C.I. (2000). Olfaction and Odor Discrimination Are Mediated by the C. elegans Guanylyl Cyclase ODR-1. Neuron *25*, 575–586.

L'Etoile, N.D., Coburn, C.M., Eastham, J., Kistler, A., Gallegos, G., and Bargmann, C.I. (2002). The Cyclic GMP-Dependent Protein Kinase EGL-4 Regulates Olfactory Adaptation in C. elegans. Neuron *36*, 1079–1089.

Li, H.-B., Mao, R.-R., Zhang, J.-C., Yang, Y., Cao, J., and Xu, L. (2008). Antistress Effect of TRPV1 Channel on Synaptic Plasticity and Spatial Memory. Biological Psychiatry *64*, 286–292.

Lindy, A.S., Parekh, P.K., Zhu, R., Kanju, P., Chintapalli, S.V., Tsvilovskyy, V., Patterson, R.L., Anishkin, A., van Rossum, D.B., and Liedtke, W.B. (2014). TRPV

channel-mediated calcium transients in nociceptor neurons are dispensable for avoidance behaviour. Nat Commun *5*, 4734.

Lovelace, J.W., Vieira, P.A., Corches, A., Mackie, K., and Korzus, E. (2014). Impaired Fear Memory Specificity Associated with Deficient Endocannabinoid-Dependent Long-Term Plasticity. Neuropsychopharmacol *39*, 1685–1693.

Madasu, M.K., Roche, M., and Finn, D.P. (2015). Supraspinal Transient Receptor Potential Subfamily V Member 1 (TRPV1) in Pain and Psychiatric Disorders. In Modern Trends in Pharmacopsychiatry, D.P. Finn, and B.E. Leonard, eds. (S. Karger AG), pp. 80–93.

Marsch, R., Foeller, E., Rammes, G., Bunck, M., Kossl, M., Holsboer, F., Zieglgansberger, W., Landgraf, R., Lutz, B., and Wotjak, C.T. (2007). Reduced Anxiety, Conditioned Fear, and Hippocampal Long-Term Potentiation in Transient Receptor Potential Vanilloid Type 1 Receptor-Deficient Mice. Journal of Neuroscience *27*, 832–839.

Minke, B. (2010). The History of the *Drosophila* TRP Channel: The Birth of a New Channel Superfamily. Journal of Neurogenetics *24*, 216–233.

Montell, C., and Rubin, G.M. (1989). Molecular characterization of the drosophila trp locus: A putative integral membrane protein required for phototransduction. Neuron *2*, 1313–1323.

Morelli, M.B., Amantini, C., Liberati, S., Santoni, M., and Nabissi, M. (2013). TRP Channels: New Potential Therapeutic Approaches in CNS Neuropathies. CNS & Neurological Disorders - Drug Targets *12*, 274–293.

Muller, C., Morales, P., and Reggio, P.H. (2019). Cannabinoid Ligands Targeting TRP Channels. Front. Mol. Neurosci. *11*, 487.

Muñoz-Lobato, F., Benedetti, K.L., Farah, F., Nordquist, S.K., Bokka, A., Brueggemann, C., Li, J., Chang, E., Varshney, A., Andersen, K., Dunn, R.L., Tsujimoto, B., Tran, A., Duong, A., Churgin, M.A., Fang-Yen, C., Kato, S., VanHoven, M.K., and L'Etoile, N.D. (2019). Sleep is required to remodel specific synapses for memory consolidation. Manuscript submitted for publication.

Nagatomo, K., Ishii, H., Yamamoto, T., Nakajo, K., and Kubo, Y. (2010). The Met268Pro Mutation of Mouse TRPA1 Changes the Effect of Caffeine from Activation to Suppression. Biophysical Journal *99*, 3609–3618.

Nilius, B. (2007). TRP channels in disease. Biochimica et Biophysica Acta (BBA) - Molecular Basis of Disease *1772*, 805–812.

Nilius, B., Vennekens, R., Prenen, J., Hoenderop, J.G., Bindels, R.J., and Droogmans, G. (2000). Whole-cell and single channel monovalent cation currents through the novel rabbit epithelial Ca2+ channel ECaC. J Physiol *527 Pt 2*, 239–248.

O'Halloran, D.M., Altshuler-Keylin, S., Lee, J.I., and L'Etoile, N.D. (2009). Regulators of AWC-Mediated Olfactory Plasticity in Caenorhabditis elegans. PLoS Genet *5*, e1000761.

Peng, G., Shi, X., and Kadowaki, T. (2015). Evolution of TRP channels inferred by their classification in diverse animal species. Molecular Phylogenetics and Evolution *84*, 145–157.

Ruggiero, R.N., Rossignoli, M.T., De Ross, J.B., Hallak, J.E.C., Leite, J.P., and Bueno-Junior, L.S. (2017). Cannabinoids and Vanilloids in Schizophrenia: Neurophysiological Evidence and Directions for Basic Research. Front. Pharmacol. *8*, 399.

Sakai, T., Sato, S., Ishimoto, H., and Kitamoto, T. (2012). Significance of the centrally expressed TRP channel painless in Drosophila courtship memory. Learning & Memory *20*, 34–40.

Sawamura, S., Shirakawa, H., Nakagawa, T., Mori, Y., and Kaneko, S. (2017). TRP Channels in the Brain. pp. 295–322.

Sims, J.R., Ow, M.C., Nishiguchi, M.A., Kim, K., Sengupta, P., and Hall, S.E. (2016). Developmental programming modulates olfactory behavior in C. elegans via endogenous RNAi pathways. ELife *5*, e11642.

Tai, Y., Feng, S., Ge, R., Du, W., Zhang, X., He, Z., and Wang, Y. (2008). TRPC6 channels promote dendritic growth via the CaMKIV-CREB pathway. Journal of Cell Science *121*, 2301—2307.

Tobin, D.M., Madsen, D.M., Kahn-Kirby, A., Peckol, E.L., Moulder, G., Barstead, R., Maricq, A.V., and Bargmann, C.I. (2002). Combinatorial Expression of TRPV Channel Proteins Defines Their Sensory Functions and Subcellular Localization in C. elegans Neurons. Neuron *35*, 307–318.

Turrigiano, G., Leslie, K.R., Desai, N.S., Rutherford, L.C., and Nelson, S.B. (1998). Activity-dependent scaling of quantal amplitude in neocortical neurons. Nature *391*, 892–896.

Tzavara, E.T., Li, D.L., Moutsimilli, L., Bisogno, T., Di Marzo, V., Phebus, L.A., Nomikos, G.G., and Giros, B. (2006). Endocannabinoids Activate Transient Receptor Potential Vanilloid 1 Receptors to Reduce Hyperdopaminergia-Related Hyperactivity: Therapeutic Implications. Biological Psychiatry *59*, 508–515.

Upadhyay, A., Pisupati, A., Jegla, T., Crook, M., Mickolajczyk, K.J., Shorey, M., Rohan, L.E., Billings, K.A., Rolls, M.M., Hancock, W.O., et al. (2016). Nicotinamide is an endogenous agonist for a C. elegans TRPV OSM-9 and OCR-4 channel. Nat Commun *7*, 13135.

Vennekens, R., Hoenderop, J.G.J., Prenen, J., Stuiver, M., Willems, P.H.G.M., Droogmans, G., Nilius, B., and Bindels, R.J.M. (2000). Permeation and Gating Properties of the Novel Epithelial Ca $^{2+}$ Channel. J. Biol. Chem. *275*, 3963–3969.

Wang, D.Y.-C., Kumar, S., and Hedges, S.B. (1999). Divergence time estimates for the early history of animal phyla and the origin of plants, animals and fungi. Proc. R. Soc. Lond. B *266*, 163–171.

White, J.G., Southgate, E., Thomson, J.N., and Brenner, S. (1986). The structure of the nervous system of the nematode C. elegans. Philosophical Transactions of the Royal Society B *314*, 1–340.

Xiao, B., Dubin, A.E., Bursulaya, B., Viswanath, V., Jegla, T.J., and Patapoutian, A. (2008). Identification of Transmembrane Domain 5 as a Critical Molecular Determinant of Menthol Sensitivity in Mammalian TRPA1 Channels. Journal of Neuroscience *28*, 9640–9651.

Zhou, J., Du, W., Zhou, K., Tai, Y., Yao, H., Jia, Y., Ding, Y., and Wang, Y. (2008). Critical role of TRPC6 channels in the formation of excitatory synapses. Nature Neuroscience *11*, 741—743.